EUROPEAN RESPIRATORY *journal*

FLAGSHIP SCIENTIFIC JOURNAL OF ERS

Early View

Original article

Spermine Promotes Pulmonary Vascular Remodelling and Its Synthase is a Therapeutic Target for Pulmonary Arterial Hypertension

Yang-Yang He, Yi Yan, Xin Jiang, Jun-Han Zhao, Zhe Wang, Tao Wu, Yong Wang, Shan-Shan Guo, Jue Ye, Tian-Yu Lian, Xi-Qi Xu, Jin-Lan Zhang, Kai Sun, Fu-Hua Peng, Yu-Ping Zhou, Yi-Min Mao, Xue Zhang, Ji-Wang Chen, Shu-Yang Zhang, Zhi-Cheng Jing

Please cite this article as: He Y-Y, Yan Y, Jiang X, *et al*. Spermine Promotes Pulmonary Vascular Remodelling and Its Synthase is a Therapeutic Target for Pulmonary Arterial Hypertension. *Eur Respir J* 2020; in press (https://doi.org/10.1183 /13993003.00522-2020).

Spermine Promotes Pulmonary Vascular Remodeling and Its Synthase is a Therapeutic Target for Pulmonary Arterial Hypertension

Yang-Yang He[1#], Yi Yan[2#], Xin Jiang[3#], Jun-Han Zhao[1], Zhe Wang[4], Tao Wu[3], Yong Wang[5], Shan-Shan Guo[6], Jue Ye[1], Tian-Yu Lian[3], Xi-Qi Xu[3], Jin-Lan Zhang[4], Kai Sun[3], Fu-Hua Peng[1], Yu-Ping Zhou[3], Yi-Min Mao[7], Xue Zhang[8], Ji-Wang Chen[9], Shu-Yang Zhang[3*], Zhi-Cheng Jing[3*]

[1] State Key Laboratory of Cardiovascular Disease and FuWai Hospital, Chinese Academy of Medical Sciences and Peking Union Medical College, Beijing, China.

[2] Department of Cardiopulmonary Circulation, Shanghai Pulmonary Hospital, Tongji University School of Medicine, Shanghai, China.

[3] Department of Cardiology and Key Laboratory of Pulmonary Vascular Medicine, Peking Union Medical College Hospital, Chinese Academy of Medical Sciences and Peking Union Medical College, Beijing, China.

[4] State Key Laboratory of Bioactive Substance and Function of Natural Medicines, Institute of Materia Medica, Chinese Academy of Medical Sciences and Peking Union Medical College, Beijing, China.

[5] Department of Respiratory and Critical Care Medicine, Beijing Shijitan Hospital, Capital Medical University, Beijing, China.

[6] Department of Biochemistry, Pharmaceutical College, Henan University, Kaifeng, Henan, China.

[7] Department of Respiratory Medicine, The First Affiliated Hospital of Henan University of Science and Technology, Luoyang, Henan, China.

[8] McKusick-Zhang Center for Genetic Medicine, State Key Laboratory of Medical Molecular Biology, Institute of Basic Medical Sciences, Chinese Academy of Medical Sciences and Peking Union Medical College, Beijing, China.

[9] Section of Pulmonary, Critical Care Medicine, Sleep and Allergy, Department of Medicine, University of Illinois at Chicago, Chicago, Illinois, USA.

[#] Drs. He, Yan and Jiang contributed equally to this work.

***Corresponding Authors**

Zhi-Cheng Jing, MD, E-mail: jingzhicheng@vip.163.com; Department of Cardiology and Key Laboratory of Pulmonary Vascular Medicine, Peking Union Medical College Hospital, Chinese Academy of Medical Sciences & Peking Union Medical College, No.1, Shuai-Fu-Yuan, Dong-Cheng District, Beijing 100730, China.

Shu-Yang Zhang, MD, E-mail: shuyangzhang103@163.com; Department of Cardiology, Peking Union Medical College Hospital, Chinese Academy of Medical Sciences & Peking Union Medical College, No.1, Shuai-Fu-Yuan, Dong-Cheng District, Beijing 100730, China.

Take home message (190-character, including spaces):

Elevated plasma spermine promotes pulmonary vascular remodeling and spermine synthase is identified as a potential therapeutic target for the pathogenesis of pulmonary arterial hypertension.

Abstract

Pathological mechanisms of pulmonary arterial hypertension (PAH) remain largely unexplored. Effective treatment of PAH remains a challenge. The aim of this study was to discover the underlying mechanism of PAH through functional metabolomics and to help develop new strategies for prevention and treatment of PAH.

Metabolomic profiling of plasma in patients with idiopathic PAH was evaluated through HPLC-MS, with spermine identified to be the most significant and validated in another independent cohort. The roles of spermine and spermine synthase (SMS) were examined in pulmonary arterial smooth muscle cells (PASMCs) and rodent models of pulmonary hypertension.

Using targeted metabolomics, plasma spermine levels were found to be higher in patients with idiopathic PAH compared to healthy controls. Spermine administration promoted proliferation and migration of PASMCs and exacerbated vascular remodeling in rodent models of pulmonary hypertension. The spermine-mediated deteriorative effect can be attributed to a corresponding upregulation of its synthase (SMS) in the pathological process. Inhibition of SMS *in vitro* suppressed platelet-derived growth factor-BB–mediated proliferation of PASMCs, and *in vivo* attenuated monocrotaline-mediated pulmonary hypertension in rats.

Plasma spermine promotes pulmonary vascular remodeling. Inhibiting spermine synthesis could be a therapeutic strategy for PAH.

Introduction

Pulmonary arterial hypertension (PAH) is a multifactorial and progressive disease characterized by a sustained increase in pulmonary vascular resistance (PVR) that ultimately leads to right ventricular failure and even death[1,2]. Pathological mechanisms of PAH are largely unexplored. Currently effective therapies for PAH are still lacking[3], and thus there is an urgent need for novel therapeutic intervention and targeted treatment of PAH[4].

Metabolomics technology is playing an increasingly important role in exploring the nature of biological systems[5–7]. In the past few years, several regulatory mechanisms underlying PAH have been studied through metabolomic analysis of lung tissues from patients with PAH and various animal models of pulmonary hypertension (PH)[8-10]. Some metabolites have been evaluated for risk stratification[11] and prognosis prediction of PAH[12]. However, it remains unknown whether these metabolites and their related enzymes are potential therapeutic targets for PAH.

Recently, a targeted metabolomics method[13] has been established with a panel of 74 small molecule metabolites involved in the core network of energy, amino acid, amine, and nucleotide metabolisms. Using this method, we performed metabolic profiling of a discovery cohort, and several dysregulated metabolic pathways were identified. Among the metabolites, spermine, a member of the polyamines[14,15], was identified as the most distinguishing molecule with a much higher level in patients with idiopathic PAH (IPAH) than in healthy controls (HCs). These findings were validated in another independent cohort, and spermine levels were positively correlated to the severity of PAH.

According to these clinical findings, it was hypothesized that spermine might play an important role in PAH by promoting pulmonary vascular remodeling, and that inhibition of spermine synthesis might attenuate PAH. To test these hypotheses, the role of spermine was examined in regulating the proliferation and migration of pulmonary arterial smooth muscle cells (PASMCs) and pulmonary vascular remodeling in rodent models of PH. Spermine synthase (SMS) is a key enzyme for spermine synthesis, and thus the effect of inactivating SMS on pulmonary vascular remodeling in experimental models of PH was evaluated.

Methods

A detailed Methods section is provided in the Supplementary Materials.

Results

Seventeen metabolites are altered in IPAH, and spermine is associated with clinical characteristics

Targeted metabolomics was adopted to assess the plasma levels of 74 small metabolites in 30 patients with IPAH and 30 matched HCs (Age: 30.4 ± 9.4 vs 34.1 ± 11.5 years; Female: 83% vs 73%)(**Supplementary Table S1** and **Table S2**). 17 metabolites with significantly changes revealed distinct metabolite profiles between HCs and IPAH patients (**Figure 1a**). 8 upregulated metabolites and 9 downregulated metabolites were found in the IPAH cohort compared to the matched HCs (fold change > 2.0 or < 0.5; $P < 0.05$) (**Supplementary Figure S1**), suggesting altered plasma metabolite profiles in PAH patients. 13 metabolic pathways, including purine, beta-alanine, arginine, and proline metabolic pathways were significantly altered in patients with IPAH (**Figure 1b** and **Supplementary Table S3**). Furthermore, according to the VIP score (**Figure 1c** and **Supplementary Figure S2a**), spermine, as the best discriminator among the 17 metabolites, was significantly higher in patients with IPAH than in HCs (**Figure 1d**). Furthermore, its upstream metabolite, arginine, was significantly lower in the IPAH group (**Supplementary Figure S2b**).

To verify these findings, liquid chromatography-mass spectrometry was used to measure plasma spermine levels in another independent validation cohort of 45 patients with IPAH and 60 matched HCs (Age: 31.8 ± 7.0 vs 28.9 ± 6.6 years; Female: 87% vs 87%) (**Supplementary Table S1**). In accordance with the discovery cohort results, spermine levels were also significantly elevated in patients with IPAH compared to the matched HCs in the validation cohort (**Figure 1d**).

To examine whether spermine was associated with clinical phenotypes, the patients were divided into high spermine group (H-group) and low spermine group (L-group) based on the median plasma spermine levels. Higher mean right atrial pressure (mRAP) and lower mixed venous oxygen saturation (SvO_2) was found in H-group (**Figure 1d**), but there was no difference in mean pulmonary arterial pressure (mPAP) and pulmonary vascular resistance (PVR) between two groups (**Supplementary Figure S3**). A tendency towards a positive correlation of spermine and mRAP and in favor of a negative correlation of spermine and SvO_2 were shown in **Supplementary Figure S4**. Moreover, spermine levels were significantly higher in IPAH patients with World Health Organization (WHO) functional classes[16] of III or IV than in those with WHO functional classes of I or II (**Figure 1d**). In addition, plasma spermine levels were also increased in rats with monocrotaline (MCT)-induced PH model, which is consistent with our human clinical data (**Supplementary Figure S5**).

Spermine promotes proliferation and migration of PASMCs

Excessive proliferation and migration of PASMCs are major pathological drivers of pulmonary vascular remodeling[17,18]. Therefore, the effect of spermine on the proliferation and migration of PASMCs was assessed. Spermine at 250 μM significantly increased proliferation and viability of rat PASMCs in response to platelet-derived growth factor-BB (PDGF-BB) stimulation (**Figure 2a, b**). The optimal concentration was determined by a cell viability assay (**Supplementary Figure S6a**). In addition, the pro-proliferative effects of spermine in response to PDGF-BB were further verified in human PASMCs using the same spermine

concentration (**Figure 3a, b**). Furthermore, proliferative effect of spermine was further validated by BrdU incorporation and cell counting assays, and we demonstrated that spermine (100 and 250 μM) significantly promoted PDGF-BB-induced proliferation in human PASMCs (**Supplementary Figure S6b, c**).

As shown in **Figure 2c** and **d**, the migration rate was significantly higher in spermine-treated rat PASMCs compared to vehicle-treated cells in response to PDGF-BB. In addition, spermine significantly promoted the migration of human PASMCs during live cell analysis using the IncuCyte S3 system that continuously assesses wound confluence (**Figure 3c, d**).

Spermine promotes progression of PH in experimental rodent models

Firstly, the optimal dose of spermine (3 mg/kg per day, intraperitoneally) was determined in a pilot study (**Supplementary Figure S7a–c**). A significant increase in right ventricular systolic pressure (RVSP), mPAP, and right ventricular hypertrophy index (RVHI) in rats that received an intraperitoneal injection of 3 mg/kg spermine following MCT administration compared with rats treated with MCT alone. This elevation was not observed in rats that received spermine following saline injection (**Figure 4a**). A similar trend in rats that received 1 mg/kg spermine after MCT challenge compared to those with MCT alone was also observed (**Supplementary Figure S8a–c**). A more severe pulmonary vascular remodeling (as measured by the ratio of the media cross-sectional area to the total vessel cross-sectional area and degree of vessel muscularization) was also observed in spermine-treated rats compared to saline-treated ones after MCT administration (**Figure 4b, c**). Consistent with observations in

the MCT-induced PH model, spermine significantly enhances the increases in RVSP, RVHI, and pulmonary arterial media thickness in the hypoxia-induced PH mouse model (**Figure 4d**).

SMS deteriorates the phenotype of PASMCs

SMS is the key enzyme that catalyzes the production of spermine from spermidine and decarboxylated S-adenosylmethionine, and plays a crucial role in maintaining homeostasis of spermine *in vivo*[19,20]. Increased SMS expression levels were observed in rat PASMC in response to PDGF-BB stimulation for 24 and 48 h compared to the control group (**Figure 5a**). Similarly, SMS expression levels in rat PASMCs were also significantly increased under hypoxic conditions compared to normoxic condition (**Figure 5b**).

To determine whether overexpression of SMS mediated PASMC pathophenotypes, human PASMCs were transfected with a recombinant adenoviral vector (**Supplementary Figure S9**) carrying the human *SMS* gene. After infection for 48 h, the infection efficiency and expression of SMS were detected by western blotting and immunofluorescence, respectively (**Figure 5c**). Overexpression of SMS increased cell viability and proliferation in response to PDGF-BB. (**Figure 5d**).

Inhibition of SMS suppresses proliferation and migration of PASMCs

5′-Deoxy-5′-methylthioadenosine (MTA), a small molecule inhibitor of SMS[19–21], produced no toxic effects at 50 μM or below (**Supplementary Figure S10a**). MTA (30 μM) significantly suppressed PDGF-BB-mediated proliferation and viability of PASMCs (**Figure 6a**). Western blotting demonstrated a marked decline in Osteopontin (OPN)[22,23] expression of

MTA-treated PASMCs in response to PDGF-BB (**Supplementary Figure S10b**). MTA also significantly inhibited the migration of PASMCs in response to PDGF-BB stimulation (**Figure 6b, c**). Furthermore, spermine levels in supernatant of PASMCs were significantly decreased after SMS inhibition (**Supplementary Figure S10c**).

Small interfering RNA (siRNA) was next used to silence the *SMS* gene. The gene-silencing efficiency was quantified by western blotting, and a marked decline in SMS expression was observed in PASMCs treated with SMS siRNA for 48 h compared with control siRNA treatment (**Figure 6d**). SMS silencing led to marked reductions in both the proliferation and viability of PASMCs in response to PDGF-BB stimulation (**Figure 6d**). In addition, the PASMC migratory ability was significantly reduced with SMS silencing compared to control PASMCs at 12 h post-treatment with PDGF-BB (**Supplementary Figure S11a**, **b**).

Modulation of the *SMS* gene alters experimental PH development

An MCT-mediated rat model was next used to assess the therapeutic potential of *SMS* gene knockdown. The knockdown efficiency was verified by western blotting, confirming that SMS expression in the lung tissues of Sprague-Dawley rats was significantly decreased after AAV-shRNA-SMS delivery (**Supplementary Figure S12**). MCT administration for 3 weeks significantly increased mPAP, RVSP, and RVHI (**Figure 7a-c**). Notably, these MCT-induced changes were prevented by SMS shRNA. The ratio of the media cross-sectional area to the total vessel cross-sectional area was also significantly lower in rats treated with MCT following AAV-shRNA-SMS administration compared to those with MCT and the control

AAV (**Figure 7d**). In order to further evaluate effects of SMS in vivo, we also examined its role in hypoxia induced PH in mice. Overexpressing SMS via tracheal delivery of recombinant human SMS-AAV significantly enhanced RVSP of mice exposure to hypoxia (**Supplementary Figure S13**).

Spermine promotes PASMC proliferation through the Erk1/2 signaling pathway

To investigate the molecular signaling pathway underlying the deleterious role of spermine in the rodent model and PASMCs in response to PDGF-BB, digital gene expression analysis of human PASMCs in the absence or presence of spermine was performed following 6 h of exposure to PDGF-BB (20 ng/mL) or vehicle (three independent biological replicates). Given that spermine treatment deteriorated PASMC phenotype after PDGF-BB stimulation, we identified genes that were differentially expressed in human PASMCs treated with spermine or vehicle in the presence or absence of PDGF-BB. Quantitative analysis and heatmap revealed 14 upregulated genes (red) and 39 downregulated genes (blue) in spermine-treated human PASMC compared to those treated with vehicle in response to PDGF-BB (fold change > 1.2; $P < 0.05$) (**Figure 8a**).

Real-time polymerase chain reaction (PCR) analysis was next used to validate 6 upregulated and 6 downregulated candidate genes according to the ranking of fold changes. The analysis confirmed increases in mRNA expression of the mitogen-activated protein kinase binding associated gene MICAL C-Terminal Like (*MICALCL*) and Transcription Factor 7 (*TCF7*) in human PASMCs exposed to PDGF-BB, which were further increased in

PASMCs treated with spermine, followed by PDGF-BB (**Figure 8a**).

MICALCL (also known as extracellular regulated protein kinase [ERK] 2-binding testicular protein 1) was defined as the most distinct gene in our validation results. MICALCL cooperates with mitogen-activated protein kinase 1/Erk2 via an intracellular signal transduction pathway during morphogenetic transformation of round spermatids to spermatozoa[24,25]. MICALCL also binds to non-phosphorylated and phosphorylated forms of Erk1/2[25,26]. Pathway enrichment analysis for differentially expressed genes using the Kyoto Encyclopedia of Genes and Genomes database demonstrated an involvement of MAPK/ERK signaling (**Supplementary Figure S14a**). It was hypothesized that spermine might mediate the phenotype of PASMCs by modulating the Erk1/2 signaling pathway. This possibility was analyzed and the expression profiles of some other pathways involved in the pathogenesis of PAH, including Akt, Smad, and Rho/MLC signaling pathways, which have been reported to be dysregulated in various animal models of PH and in patients with PAH[27–30]. As shown in **Figure 8b**, PASMCs exposed to spermine exhibited higher phosphorylation of Erk1/2 compared with control PASMCs after PDGF-BB stimulation for 2 h. In contrast, spermine did not significantly increase phosphorylation of Akt, MLC, or Smad2 in PASMCs in response to PDGF-BB (**Supplementary Figure S14b-e**).

Western blot analysis confirmed marked upregulation of Erk1/2 phosphorylation in response to PDGF-BB in PASMCs treated with spermine, which was restored to a level similar to that in normal PASMCs after Selumetinib (AZD6244, a potent Erk1/2 phosphorylation inhibitor[31,32]) treatment (**Figure 8c**). Furthermore, AZD6244 significantly suppressed human and rat PASMC proliferation after stimulation by PDGF-BB in the

presence or absence of spermine. Suppression was similar regardless of whether spermine was present (**Figure 8c** and **Supplementary Figure S15)**.

Discussion

In this study, targeted metabolomics technology was employed to examine plasma samples isolated from two independent IPAH cohorts. We first demonstrated that plasma spermine levels are significantly elevated in patients with IPAH. We also found that spermine promotes PASMC proliferation and migration in an Erk-dependent manner and exacerbates pulmonary vascular remodeling in two rodent models of PH. Inhibition of SMS attenuates PDGF-BB-mediated PASMC proliferation and migration. Furthermore, silencing SMS expression attenuates pulmonary vascular remodeling in the experimental model of PH. Our study clearly demonstrates that spermine promotes pulmonary vascular remodeling and inhibition of spermine synthesis may have therapeutic effects in patients with PAH.

As a polyamine, spermine associates with nucleic acids to stabilize the nucleic acid helical structure and is involved in cellular metabolism of all eukaryotic cells[33,34]. Regulation of polyamine transport and import has been well studied in pulmonary artery endothelial cells during the past decades[35,36]. In addition, a previous exploratory study demonstrated an elevation of spermine in lung tissues from a rat model MCT-induced PH[37]. However, up to now there has been no report regarding the elevated plasma level of spermine in humans. In

this study, we confirmed the deleterious effect of spermine on the development of PH *in vivo* and its pro-proliferative and pro-migratory capacity in PASMCs *in vitro*, although a previous study showed an anti-proliferative effect on human PASMCs after a chemical induced hypoxia condition[38]. This disparity might be attributable to the use of different cell culture models, and the chemical stabilizer of hypoxia-inducible factor cobalt chloride in some circumstances might fail to increase nuclear hypoxia-inducible factor-1α protein levels[39]. In addition, the transcription of distinct sets of genes induced by cobalt chloride that were not affected by cellular hypoxia suggests caution in the use of hypoxia mimics as substitutes for the low O_2 tension[40].

For the past two decades, elevated spermine levels have been increasingly reported in malignant and proliferating cells [41,42]. Metabolism of polyamines is frequently dysregulated in patients with cancer or other hyperproliferative diseases, thus making polyamine function and metabolism attractive targets for risk stratification and therapeutic intervention[43,44]. L-arginine, the upstream molecule of arginine-nitric oxide (NO) and polyamine metabolism, is involved in the regulation of vascular homeostasis, including pulmonary vascular tone and proliferation[45,46]. It is also downregulated in lung tissues and plasma of IPAH patients[47,48]. Prolonged administration of L-arginine alleviates vascular remodeling in rats with chronic hypoxia- or MCT-induced PH[49]. Oral supplementation with L-arginine also elicits beneficial effects on hemodynamics and exercise capacity in patients with precapillary PAH[48]. In the current metabolomic analysis, we observed significant reduction of plasma L-arginine levels in patients with IPAH, which supports our metabolite detection methodology. The significant increase in spermine, a polyamine[33] downstream of the arginine-arginase-ornithine metabolic

pathway[50], may be at least partially responsible for the arginine deficiency observed in patients with IPAH. As a result, NO production decreases and vessel contraction increases.

SMS, a specific aminopropyl transferase, acts directly to generate spermine from spermidine and decarboxylated S-adenosylmethionine. The crystal structure of human SMS and its catalytic mechanism have been determined previously[51]. Recognition that dysregulated spermine is required for tumorigenesis led to the development of inhibitors for each step of spermine biosynthesis or catabolism[52]. Spermine depletion using an SMS inhibitor has been investigated as a potential therapy in various types of cancer, including human breast cancer, hepatoma, and pancreatic cancer[53–55]. It is well known that the pathobiology of PAH shares many similar features with tumorigenesis, which may help develop novel therapeutic strategies for PAH[56]. Consistent with these previous findings, our results suggest that SMS inhibition may be a potential therapeutic strategy for PAH. The intricate regulatory mechanisms of polyamine homeostasis, involving biosynthesis, catabolism and transmembrane transportation, warrant further investigations to assess its potential as a therapeutic approach.

In our metabolic study, spermine displayed no relationship with bilirubin (shown in **Supplementary Figure S16a**), although another study by Rhodes et al. showed bilirubin correlated with another polyamine metabolites (4-acetamidobutanoate and N-acetylputrescine), which were also increased in PAH and prognostic in PAH cohorts[12]. This suggests that spermine may play a different role in PAH compared to other polyamines. However, we found MTA (another polyamine metabolite) had a positive correlation with spermine (P = 0.0071), as evident in **Supplementary Figure S16b**. Although MTA is

identified as an SMS inhibitor that occurs naturally *in vivo*, but it's not stable in the body and easily degraded by its phosphatase[19-21]. In addition, it can also inhibit adenosine receptors, methyltransferases and other targets. Taken together, specific SMS inhibitors with higher stability should warrant our further studies.

Emerging evidence has shown that Erk1/2 signaling is critical for regulating cell fate commitment[57,58], and that Erk1/2 pathways are activated in the pulmonary vasculature of patients with PAH[59]. Furthermore, PAH is mainly characterized by excessive proliferation of PASMCs (partially due to activation of Erk1/2 signaling[60,61]). Since MICALCL is a downstream molecule that interacts with Erk2 and participates in the intracellular signal transduction pathway[25,26], spermine promoted PASMC proliferation in an Erk signaling-dependent fashion, and the inhibition of Erk signaling rescued the effect of spermine on PASMCs.

Collectively, our human plasma-based metabolomics approach and subsequent experiments in PASMCs and rodent models of PH demonstrate the detrimental role of dysregulated spermine in the pathogenesis of PAH. The underlying mechanism mediated by spermine involves modulation of the Erk1/2 signaling pathway, which promotes PASMC proliferation and pulmonary vascular remodeling (**Figure 8d**). Inhibiting the synthesis of spermine via targeting SMS or other genes in the downstream signaling pathway of spermine could be novel potential therapeutic strategies for PAH.

Funding

This work was supported by grants from the National Natural Science Foundation of China (81630003, 81700059), 13th Five-Year Plan - Precision Medicine - Key Research and Development Program - Clinical Cohort of Rare Disease (2016YFC0901500), Beijing Natural Science Foundation (7181009, 7182139), CAMS Innovation Fund for Medical Sciences (2016-I2M-1-002, 2017-I2M-BR-02, 2017PT32016, 2017-I2M-1-004, 2017-I2M-1-011, 2017-I2M-2-001).

Acknowledgments

The authors gratefully thank the patients and families for their involvement in this study.

Conflict of interest

None.

References

1. Humbert M, et al. Risk assessment in pulmonary arterial hypertension and chronic thromboembolic pulmonary hypertension. *Eur. Respir. J.* **6**, pii: 1802004. (2019).

2. Galiè, N. et al. 2015 ESC/ERS Guidelines for the diagnosis and treatment of pulmonary hypertension: The Joint Task Force for the Diagnosis and Treatment of Pulmonary Hypertension of the European Society of Cardiology (ESC) and the European Respiratory Society (ERS): Endorsed by: Association for European Paediatric and Congenital Cardiology (AEPC), International Society for Heart and Lung Transplantation (ISHLT). *Eur. Heart J.* **1**, 67–119 (2015).

3. Hoeper M, The new haemodynamic definition of pulmonary hypertension: evidence prevails, finally! *Eur. Respir. J.* **3**, pii: 1900038. (2019).

4. Chen, J. et al. The sphingosine kinase 1/sphingosine-1-phosphate pathway in pulmonary arterial hypertension. *Am. J. Respir. Crit. Care Med.* **9**, 1032–1043 (2014).

5. Beger, R. D. et al. Metabolomics enables precision medicine: "a white paper, community perspective". *Metabolomics* **10**, 149 (2016).

6. Rhee, K. Minding the gaps: metabolomics mends functional genomics. *EMBO Reports* **1**, (2013).

7. Lewis, G. D. The emerging role of metabolomics in the development of biomarkers for pulmonary hypertension and other cardiovascular diseases (2013 Grover Conference series). *Pulm. Circ.* **3**, 417–423 (2014).

8. Li, M. et al. Metabolic reprogramming regulates the proliferative and inflammatory phenotype of adventitial fibroblasts in pulmonary hypertension through the transcriptional corepressor C-terminal binding protein-1. *Circulation* **134**, 1105–1121 (2016).

9. Talati, M. H. et al. Mechanisms of lipid accumulation in the bone morphogenetic protein receptor type 2 mutant right ventricle. *Am. J. Respir. Crit. Care Med*. **6**, 719–728 (2016).

10. Zhao, Y. D. et al. De novo synthesize of bile acids in pulmonary arterial hypertension lung. *Metabolomics* **6**, 1169–1175 (2014).

11. Lewis, G. D. et al. Metabolic profiling of right ventricular-pulmonary vascular function reveals circulating biomarkers of pulmonary hypertension. *J. Am. Coll. Cardiol.* **2**, 174–189 (2016).

12. Rhodes, C. J. et al. Plasma metabolomics implicate modified transfer RNAs and altered

bioenergetics in the outcome of pulmonary arterial hypertension. *Circulation* **5**, 460–475 (2017).

13. Wang, Z., Zhang, J., Ren, T., & Dong, Z. Targeted metabolomic profiling of cardioprotective effect of Ginkgo biloba L. extract on myocardial ischemia in rats. *Phytomedicine* **6**, 621–631 (2016).

14. Matthews, H. R. My favourite molecule: Polyamines, chromatin structure and transcription. *Bioessays* **8**, 561–566 (1993).

15. Tabor, H. & Tabor, C. W. Spermidine, spermine, and related amines. *Pharmacol. Rev*. **3**, 245–300 (1964).

16. Bennett, J. A. et al. Validity and reliability of the NYHA classes for measuring research outcomes in patients with cardiac disease. *Heart Lung* **4,** 262–270 (2002).

17. Morrell, N. W. et al. Cellular and molecular basis of pulmonary arterial hypertension. *J. Am. Coll. Cardiol*. **1**, S20–S31 (2009).

18. Yuan, J. X. J. et al. Dysfunctional voltage-gated K^+ channels in pulmonary artery smooth muscle cells of patients with primary pulmonary hypertension. *Circulation* **14**, 1400–1406 (1998).

19. Hibasami, H. et al. Studies of inhibition of rat spermidine synthase and spermine synthase. *Biochem. J*. **2**, 419–428 (1980).

20. Pegg, A. E. & Michael, A. J. Spermine synthase. *Cell Mol. Life. Sci*. **1**, 113–121 (2010).

21. Pajula, R. L. & Raina, A. Methylthioadenosine, a potent inhibitor of spermine synthase from bovine brain. *FEBS. Lett*. **2**, 343–345 (1979).

22. Jie, W. et al. Contribution of myocardin in the hypoxia-induced phenotypic switching of rat pulmonary arterial smooth muscle cells. *Exp. Mol. Pathol*. **3**, 301–306 (2010).

23. Peng, X. et al. Involvement of calcium-sensing receptors in hypoxia-induced vascular remodeling and pulmonary hypertension by promoting phenotypic modulation of small pulmonary arteries. *Mol. Cell Biochem*. **1–2**, 87–98 (2014).

24. Amrita R. et al. bMERB domains are bivalent Rab8 family effectors evolved by gene duplication. *eLife* **5**, e18675 (2016).

25. Miura, K. ERK2-binding domain is required for phosphorylation of EBITEIN1, a potential downstream interactor of ERK2. *Biochem. Biophys. Res. Commun*. **3**, 367–371 (2008).

26. Miura, K. & Imaki, J. Identification of ERK2-binding domain of EBITEIN1, a novel ERK2-binding protein. *Biochim. Biophys. Acta*. **9**, 1319–1325 (2008).

27. Schermuly, R. T. et al. Reversal of experimental pulmonary hypertension by PDGF inhibition. *J. Clin. Invest.* **10**, 2811–2821 (2005).

28. Datta, K., Bellacosa, A., Chan, T. O. & Tsichlis, P. N. Akt is a direct target of the phosphatidylinositol 3-kinase. Activation by growth factors, v-src and v-Ha-ras, in Sf9 and mammalian cells. *J. Biol. Chem.* **48**, 30835–30839 (1996).

29. Yang, X. et al. Dysfunctional Smad signaling contributes to abnormal smooth muscle cell proliferation in familial pulmonary arterial hypertension. *Cir. Res.* **10**, 1053–1063 (2005).

30. Oka, M., Fagan, K. A., Jones, P. L. & McMurtry, I. F. Therapeutic potential of RhoA/Rho kinase inhibitors in pulmonary hypertension. *Br. J. Pharmacol.* **4**, 444–454 (2008).

31. Yeh, T. C. et al. Biological characterization of ARRY-142886 (AZD6244), a potent, highly selective mitogen-activated protein kinase 1/2 inhibitor. *Clin. Cancer. Res.* **5**, 1576–1583 (2007).

32. Friday, B. B. & Adjei, A. A. Advances in targeting the Ras/Raf/MEK/Erk mitogen-activated protein kinase cascade with MEK inhibitors for cancer therapy. *Clin. Cancer Res.* **2**, 342–346 (2008).

33. Morgan, D. M. L. Polyamines. *Mol. Biotechnol*. **3**, 229–250 (1999).

34. Balasundaram, D. & Tyagi, A. K. Polyamine-DNA nexus: structural ramifications and biological implications. *Mol. Cell. Biochem.* **2**, 129–140 (1991).

35. Babál P. et al. Regulation of ornithine decarboxylase activity and polyamine transport by agmatine in rat pulmonary artery endothelial cells. *J. Pharmacol. Exp. Ther.* **2**, 372-377 (2001).

36. Babal P. et al. Regulation of ornithine decarboxylase and polyamine import by hypoxia in pulmonary artery endothelial cells. *Am. J. Physiol. Lung Cell Mol. Physiol*. **4**, L840-L846 (2002).

37. Orlinska U. et al. Polyamine content in pulmonary arteries from rats with monocrotaline-induced pulmonary hypertension. *Res. Commun. Chem. Pathol. Pharmacol.* **2**, 187-194(1988).

38. Wei C. et al. Exogenous spermine inhibits the proliferation of human pulmonary artery smooth muscle cells caused by chemically-induced hypoxia via the suppression of the ERK1/2- and PI3K/AKT-associated pathways. *Int. J. Mol. Med.* **1**, 39-46(2016).

39. Groenman F. et al. Effect of chemical stabilizers of hypoxia-inducible factors on early lung development. *Am. J. Physiol. Lung Cell Mol. Physiol.* **3**, L557-L567(2007).

40. Vengellur A. et al. Gene expression profiling of hypoxia signaling in human hepatocellular carcinoma cells. *Physiol. Genomics.***3**, 308-318(2005).

41. Amendola, R. et al. Spermine metabolism and anticancer therapy. *Curr. Cancer Drug Targets* **2**, 118–130 (2009).

42. Gillespie M.N., Olson J.W. Polyamine regulatory pathways as pharmacologic targets in pulmonary arterial hypertension. *Adv. Exp. Med. Biol.* 375-389 (2010).

43. Casero Jr., R. A. & Woster, P. M. Recent advances in the development of polyamine analogues as antitumor agents. *J. Med. Chem.* **15**, 4551–4573 (2009).

44. Casero Jr, R. A. & Marton, L. J. Targeting polyamine metabolism and function in cancer and other hyperproliferative diseases. *Nat. Rev. Drug Discov.* **5**, 373–390 (2007).

45. Palmer, R. M. J., Ashton, D. S., & Moncada, S. Vascular endothelial cells synthesize nitric oxide from L-arginine. *Nature* **6174**, 664–666 (1988).

46. Dinh-Xuan, A. T. Endothelial modulation of pulmonary vascular tone. *Eur. Respir J.* **6**, 757–762 (1992).

47. Mehta, S. et al. Short-term pulmonary vasodilation with L-arginine in pulmonary hypertension. *Circulation* **6**, 1539–1545 (1995).

48. Nagaya, N. et al. Short-term oral administration of L-arginine improves hemodynamics and exercise capacity in patients with precapillary pulmonary hypertension. *Am. J. Respir. Crit. Care Med.* **4**, 887–891 (2001).

49. Mitani, Y., Maruyama, K. & Sakurai, M. Prolonged administration of L-arginine ameliorates chronic pulmonary hypertension and pulmonary vascular remodeling in rats. *Circulation* **2**, 689–697 (1997).

50. Pegg, A. E. Polyamine metabolism and its importance in neoplastic growth and as a target for chemotherapy. *Cancer Res.* **4**, 759–774 (1988).

51. Wu, H. et al. Crystal structure of human spermine synthase implications of substrate binding and catalytic mechanism. *J. Biol. Chem.* **23**, 16135–16146 (2008).

52. Pegg, A. E. The function of spermine. *IUBMB. Life* **1**, 8–18 (2014).

53. Huber, M. & Poulin, R. Antiproliferative effect of spermine depletion by N-cyclohexyl-1,

3-diaminopropane in human breast cancer cells. *Cancer Res*. **4**, 934–943 (1995).

54. Beppu, T. et al. Specific depletion of spermidine and spermine in HTC cells treated with inhibitors of aminopropyltransferases. *J. Biochem*. **2**, 339–345 (1995).

55. Massaro, C., Thomas, J. & Phanstiel IV, O. Investigation of polyamine metabolism and homeostasis in pancreatic cancers. *Med. Sci*. **4**, 32 (2017).

56. Guignabert, C. et al. Pathogenesis of pulmonary arterial hypertension: lessons from cancer. *Eur. Respir. Rev*. **130**, 543–551 (2013).

57. Chen, K. H. et al. Epigenetic dysregulation of the Drp1 binding partners MiD49 and MiD51 increases mitotic mitochondrial fission and promotes pulmonary arterial hypertension: Mechanistic and therapeutic implications. *Circulation* **138**, 287–304 (2018)

58. Awad, K. S. et al. Raf/ERK drives the proliferative and invasive phenotype of BMPR2-silenced pulmonary artery endothelial cells. *Am. J. Physiol. Lung Cell Mol. Physiol*. **310**, L187–L201 (2015).

59. Lei, W. et al. Expression and analyses of the HIF-1 pathway in the lungs of humans with pulmonary arterial hypertension. *Mol. Med. Rep*. **14**, 4383–4390 (2016).

60. Hansmann, G. et al. An antiproliferative BMP-2/PPARγ/apoE axis in human and murine SMCs and its role in pulmonary hypertension. *J. Clin. Invest*. **118**, 1846–1857 (2008).

61. Kovacs L., Cai, P. & Su, Y. Inhibitory role of BMP4 on the PDGF-induced proliferation and collagen synthesis in PASMCs. *FASEB. J.* **31**, lb653–lb653 (2017).

Figure legends

Figure 1 Metabolites distinguishing pulmonary arterial hypertension (PAH) and healthy controls (HCs) identified by targeted metabolomics. (**a**) Heat map generated from liquid chromatography-mass spectrometry of the discovery cohort, showing differences in the metabolite signatures of HCs and patients with idiopathic PAH (IPAH). Each column represents an individual sample from each group. A total of 17 metabolites were significantly upregulated (red) or downregulated (blue) in the plasma of IPAH patients compared with HCs. The color intensity is proportional to the fold change of the ratio, and the numbers represent numerization. (**b**) The most relevant pathways were identified by pathway enrichment and topology analyses. (**c**) Ranking of differentiating metabolites was based on the VIP score. (**d**) Spermine levels (after base 10 log transformation) in the plasma of HCs and patients with IPAH in the discovery cohort (n = 30 per group) and validation cohort (n = 60 for HC and n = 45 for IPAH patients). ***P < 0.001, **P < 0.01; Mann–Whitney U test and Student's t-test. Data are presented as box-and-whisker plots with scatter (box center line = median value, box = interquartile range, and whiskers = lowest and highest values). Hemodynamic parameters, including mean right atrial pressure (mRAP), and mixed venous oxygen saturation (SvO_2), exhibited significant differences between high (n = 22) and low (n = 23) spermine groups divided by the median value. **P < 0.01, *P < 0.05; Student's t-test. Data are presented as box-and-whisker plots with scatter. Spermine levels (after base 10 log transformation) in the plasma of patients with IPAH according to the World Health Organization (WHO) functional classification in the validation cohort (n = 14 for WHO class I+II group, n = 30 for WHO

class III+V group). *$P < 0.05$; Student's *t*-test. Data are presented as box-and-whisker plots with scatter.

Figure 2 Effects of spermine on rat pulmonary arterial smooth muscle cells (PASMCs). (**a**) Effects of spermine (250 μM) on the proliferation of rat PASMCs treated with or without platelet-derived growth factor-BB (PDGF-BB) for 24 and 48 h (n = 6 per group). ***P < 0.001; one-way analysis of variance (ANOVA), Tukey's post-hoc test. The values were normalized to the control condition at each time point. Data are means ± s.e.m. (**b**) Effects of 250 μM spermine on cell viability of rat PASMCs treated with or without PDGF-BB for 24 and 48 h (n = 6 per group). ***P < 0.001; one-way ANOVA, Tukey's post-hoc test. The values were normalized to the control condition at each time point. Data are the mean ± s.e.m. (**c**) Representative bright field images obtained at ×100 magnification at 0, 24 and 48 h post-scratching. Two to three images of each individual scratch were obtained during the wound scratch assay. The results indicated that spermine (250 μM) facilitated PDGF-BB-induced PASMC migration. Scale bar, 200 μm. (**d**) Quantitative assessments of spermine-induced migration rates of rat PASMCs treated with or without PDGF-BB for 48 h (n = 10 for control group, n = 10 for spermine group, n = 14 for PDGF-BB group, and n = 15 for PDGF-BB + spermine group). ***P < 0.001; one-way ANOVA, Tukey's post-hoc test. Data are the mean ± s.e.m.

Figure 3 Effects of spermine on human pulmonary arterial smooth muscle cells (PASMCs). (**a, b**) Effects of spermine (250 μM) on cell proliferation (**a**) and viability (**b**) of human PASMCs treated with or without PDGF-BB for 48 h (n = 6 per group). $^{**}P < 0.01$, $^{***}P < 0.001$; one-way ANOVA, Tukey's post-hoc test. Data are the mean ± s.e.m. (**c**) Representative images at 0, 6, 12, and 18 h after scratching monolayers using a 96-Well Wound Maker apparatus. (**d**) Real-time kinetic curve of wound confluency induced by spermine in human PASMC cultures treated with or without PDGF-BB for 1–18 h (n = 6 per group). $^{***}P < 0.001$; two-way repeated measures ANOVA. Data are the mean ± s.e.m.

Figure 4 Spermine exacerbates the progression of pulmonary arterial hypertension in rodents after exposure to monocrotaline (MCT) or hypoxia. (**a**) Sprague-Dawley rats treated with spermine exhibited higher right ventricular systolic pressure (RVSP), mean pulmonary arterial pressure (mPAP), and right ventricular hypertrophy index [RVHI; ratio of the right ventricular weight to the left ventricular (LV) plus septal (S) weight] at Day 21 after MCT subcutaneous injection compared with rats treated with MCT alone (n = 8 for control, n = 7 for spermine group, n = 18 for MCT group, and n = 14 for MCT + spermine group). *P < 0.05, **P < 0.01, ***P < 0.001; one-way ANOVA, Tukey's post-hoc test. Data are the mean ± s.e.m. (**b**) Representative photomicrographs of hematoxylin and eosin (H&E) staining, immunofluorescence of α-SMA (red; smooth muscle cells) and anti-von Willebrand factor (green; endothelial cells), and 4′,6-diamidino-2-phenylindole (DAPI) staining (blue; nuclei) of lung tissues from MCT- or saline-treated rats at Day 21. Scale bars, 50 μm. Assessment of pulmonary vascular remodeling by the ratio of the vascular media cross-sectional area to the total vessel cross-sectional area in each group of rats (n = 4 for control group, n = 4 for spermine group, n = 5 for MCT group, and n = 5 for MCT + spermine group). *P < 0.05; one-way ANOVA, Tukey's post-hoc test. Data are the mean ± s.e.m. (**c**) Proportions of nonmuscularized (NM), partially muscularized (PM), and fully muscularized (FM) pulmonary arterioles (25–100 μm in diameter) in the lung tissues of MCT-treated rats (n = 4 for control group, n = 4 for spermine group, n = 5 for MCT group, and n = 5 for MCT + spermine group). *P < 0.05, ***P < 0.001; one-way ANOVA, Tukey's post-hoc test. Data are mean ± s.e.m. (**d**) C57BL/6 mice treated with spermine exhibited elevations in RVSP (n = 11 for control, n = 12 for spermine group, n = 9 for hypoxia group, and n = 11 for hypoxia + spermine group) and

RVHI (n = 11 for control, n = 12 for spermine group, n = 12 for hypoxia group, and n = 12 for hypoxia + spermine group) at Day 28 after hypoxic exposure compared with the normoxia group. *P < 0.05, **P < 0.01, ***P < 0.001; one-way ANOVA, Tukey's post-hoc test. Data are the mean ± s.e.m. Representative photomicrographs of H&E staining of lung tissues from mice maintained under normoxic or hypoxic conditions at Day 28. Scale bars, 50 μm. Assessment of pulmonary vascular remodeling by the percentage of the vascular medial thickness to the total vessel size in each group (n = 3 for control, n = 3 for spermine group, n = 7 for hypoxia group, and n = 6 for hypoxia + spermine group). *P < 0.05, ***P < 0.001; one-way ANOVA, Tukey's post-hoc test. Data are the mean ± s.e.m.

Figure 5 Expression of spermine synthase (SMS) in pulmonary arterial smooth muscle cells (PASMCs) and effects of SMS overexpression on the PASMC phenotype. (**a**) Quantification of SMS expression by western blotting in rat PASMCs treated with or without platelet-derived growth factor-BB (PDGF-BB) for 24 h (n = 3 per group) and 48 h (n = 4 per group). *P < 0.05; Student's t-test. Data are the mean ± s.e.m. (**b**) Quantification of SMS expression by western blotting in rat PASMCs under normoxia (21% O_2) or hypoxia (10% O_2) for 48 h (n = 4 per group). **P < 0.01; Student's t-test. Data are the mean ± s.e.m. (**c**) SMS expression was evaluated by western blotting at 48 h after control adenovirus (Ad-Ctrl) or SMS overexpressing adenovirus (Ad-SMS) infection at a multiplicity of infection (MOI) of 10 in human PASMCs. Representative photomicrographs of immunofluorescence staining of human PASMCs at 48 h after Ad-Ctrl or Ad-SMS infection (MOI = 10). Scale bars, 200 μm. (**d**) Cell proliferation and viability of human PASMCs after infection by either Ad-Ctrl or Ad-SMS at the indicated MOI for 36 h, followed by treatment with human PDGF-BB (20 ng/mL) or the vehicle for 48 h (n = 6 per group). *P < 0.05, **P < 0.01, ***P < 0.001; one-way ANOVA, Tukey's post-hoc test. Data are the mean ± s.e.m.

Figure 6 Effects of pharmacological inhibition and gene silencing of spermine synthase (SMS) on the phenotypes of pulmonary arterial smooth muscle cells (PASMCs). (**a**) Cell proliferation of rat PASMCs stimulated with platelet-derived growth factor-BB (PDGF-BB) for 24 and 48 h and cell viability of rat PASMCs stimulated with PDGF-BB for 24 h in the presence or absence of SMS inhibitor MTA (30 μM) (n = 6 per group). $^{**}P < 0.01$, $^{***}P < 0.001$; one-way ANOVA, Tukey's post-hoc test. Data are the mean ± s.e.m. (**b**) Representative images obtained at 0, 24, and 48 h post-scratching showing the effects of MTA (30 μM) on PDGF-BB (50 ng/mL)-induced migration during the wound healing assay. Scale bars, 200 μm. (**c**) Quantification of the migration rate of rat PASMCs treated with the vehicle (n = 9) or PDGF-BB in the presence of MTA (n = 8) or absence of MTA (n = 6). $^{*}P < 0.05$, $^{***}P < 0.001$; one-way ANOVA, Tukey's post-hoc test. Data are the mean ± s.e.m. (**d**) Small interfering RNA (siRNA) knockdown efficiency in PASMCs examined by immunoblotting of SMS following treatment with either SMS-specific siRNA (si*SMS*) or a pooled siRNA control (si*CP*). Cell proliferation and cell viability of rat PASMCs transfected with si*CP* or si*SMS* stimulated by PDGF-BB or the vehicle for 48 h (n = 6 per group). $^{***}P < 0.001$; one-way ANOVA, Tukey's post-hoc test. Data are the mean ± s.e.m.

Figure 7 Effects of gene silencing of spermine synthase (SMS) on monocrotaline (MCT)-induced pulmonary hypertension rats. (**a**–**c**) Sprague-Dawley rats treated with a recombinant adeno-associated virus 6 carrying SMS short hairpin RNA (AAV-shRNA-SMS) exhibited lower (**a**) mean pulmonary artery pressure (mPAP), (**b**) right ventricular systolic pressure (RVSP), and (**c**) right ventricular hypertrophy index (RVHI) compared with rats treated with the control adeno-associated virus (AAV-ctrl) (n = 12 for AAV-ctrl group, n = 12 for AAV-shRNA-SMS group, n = 11 for MCT + AAV-ctrl group, and n = 13 for MCT + AAV-shRNA-SMS group). *P < 0.05, **P < 0.01, ***P < 0.001; one-way ANOVA, Tukey's post-hoc test. Data are the mean ± s.e.m. (**d**) Representative photomicrographs of hematoxylin and eosin (H&E) staining of lung tissues from MCT or saline-treated rats. Scale bars, 50 μm. Assessment of pulmonary vascular remodeling by determination of the ratio of the media cross-sectional area to the total vessel cross-sectional area in each group (n = 5 for AAV-ctrl group, n = 5 for AAV-shRNA-SMS group, n = 4 for MCT + AAV-ctrl group, and n = 5 for MCT + AAV-shRNA-SMS group). ***P < 0.001; one-way ANOVA, Tukey's post-hoc test. Data are the mean ± s.e.m.

Figure 8 Spermine promotes proliferation of pulmonary arterial smooth muscle cells (PASMCs) through the Erk1/2 signaling pathway. (**a**) Heat map showing a subset of genes differentially expressed in human PASMCs treated with platelet-derived growth factor-BB (PDGF-BB) or the vehicle in the presence or absence of spermine for 6 h. mRNA expression of six upregulated genes and six downregulated genes was validated by real-time PCR in human PASMCs treated with or without spermine after PDGF-BB stimulation (n = 3 per group). **P* < 0.05, ***P* < 0.01, ****P* < 0.001; one-way ANOVA, Tukey's post-hoc test. Data are the mean ± s.e.m. (**b**) Effects of spermine on phosphorylation of Erk1/2 in PASMCs in the presence or absence of PDGF-BB, as determined by western blotting. Quantification of Erk1/2 phosphorylation in PASMCs, which was normalized to total Erk, as determined by scanning densitometry using the Quantity One 1-D analysis system (*n* = 4 per group). **P* < 0.05, ***P* < 0.01; one-way ANOVA, Tukey's post-hoc test. Data are the mean ± s.e.m. (**c**) Representative western blotting showing the effects of spermine on Erk phosphorylation in PASMCs in the presence or absence of AZD6244 after PDGF-BB stimulation for 2 h and its corresponding quantification (*n* = 4 per group). ***P* < 0.01, ****P* < 0.001; one-way ANOVA, Tukey's post-hoc test. Data are the mean ± s.e.m. Effects of spermine on PASMC proliferation in the presence or absence of Erk1/2 phosphorylation inhibitor AZD6244 (5 μM) after PDGF-BB (20 ng/mL) stimulation for 48 h (*n* = 6 per group). **P* < 0.05, ****P* < 0.001; one-way ANOVA, Tukey's post-hoc test. Data are the mean ± s.e.m. (**d**) Conceptual representation of the role of spermine in exacerbating vascular remodeling in PAH.

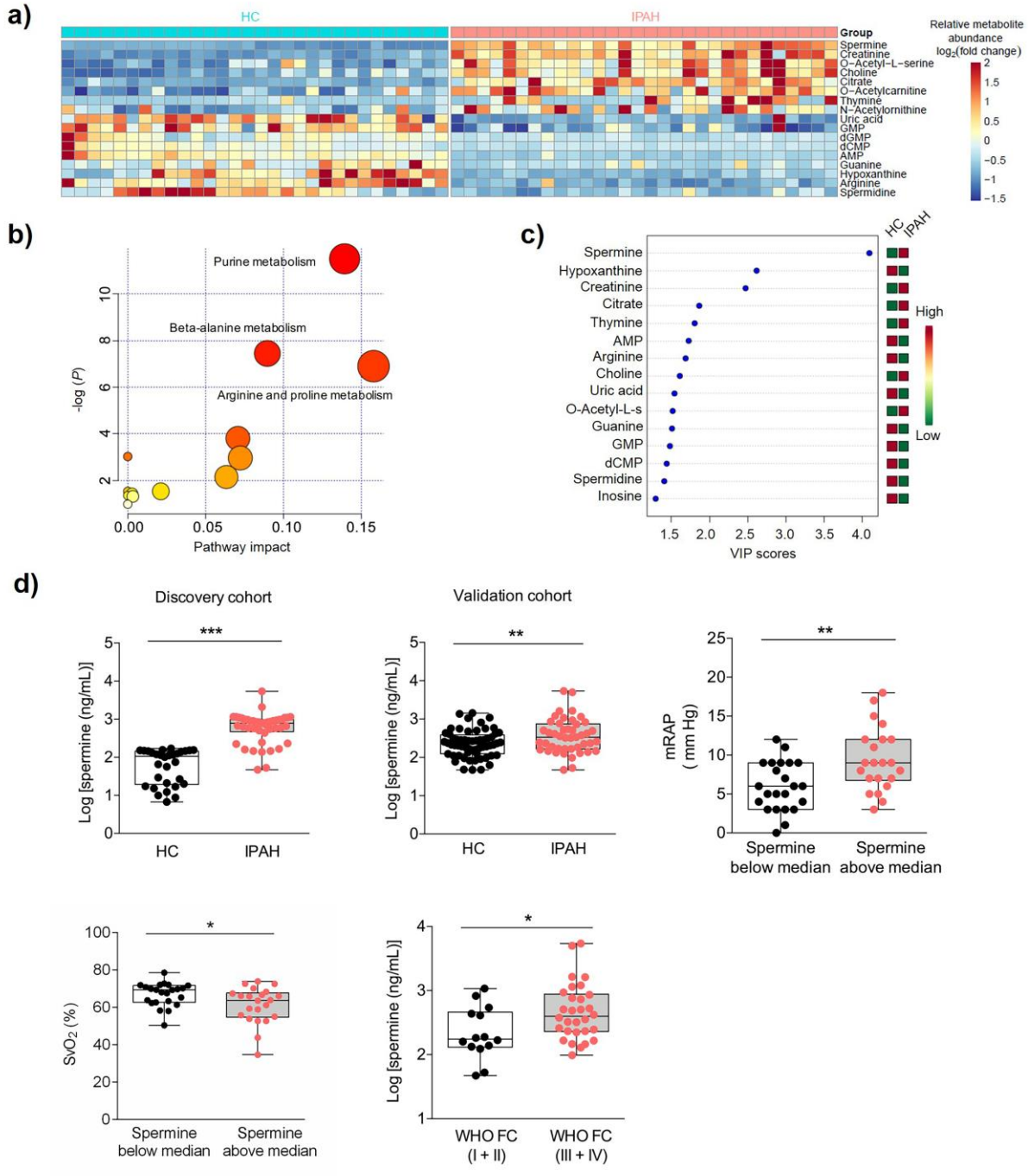
a)
HC
IPAH
Group
Spermine
Creatinine
O−Acetyl−L−serine
Choline
Citrate
O−Acetylcarnitine
Thymine
N−Acetylornithine
Uric acid
GMP
dGMP
dCMP
AMP
Guanine
Hypoxanthine
Arginine
Spermidine
Relative metabolite abundance log2(fold change)
2
1.5
1
0.5
0
−0.5
−1
−1.5
b)
Purine metabolism
Beta-alanine metabolism
Arginine and proline metabolism
-log (P)
Pathway impact
c)
HC
IPAH
Spermine
Hypoxanthine
Creatinine
Citrate
Thymine
AMP
Arginine
Choline
Uric acid
O-Acetyl-L-s
Guanine
GMP
dCMP
Spermidine
Inosine
High
Low
VIP scores
d)
Discovery cohort
Validation cohort
Log [spermine (ng/mL)]
HC
IPAH
mRAP (mm Hg)
Spermine below median
Spermine above median
SvO2 (%)
WHO FC (I + II)
WHO FC (III + IV)

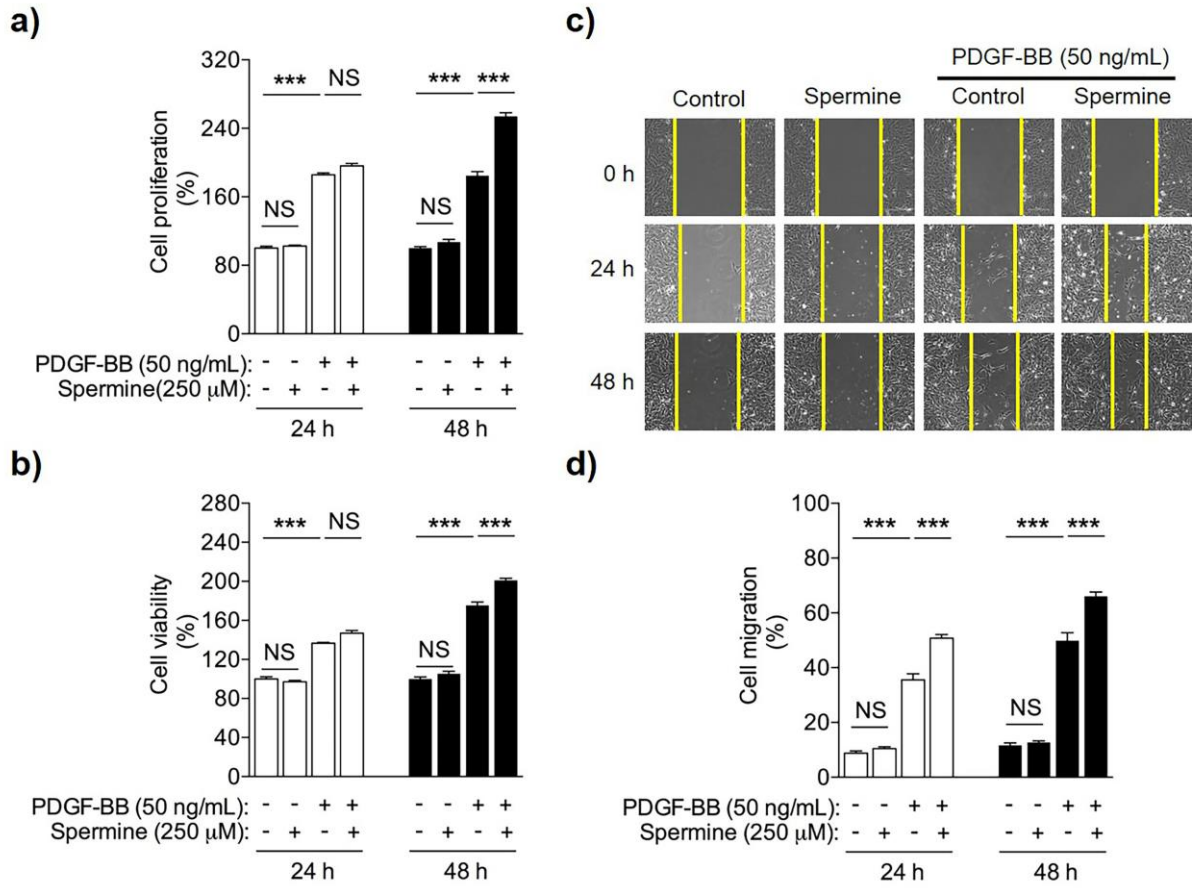
a)
Cell proliferation (%)
320
240
160
80
0
***
NS
***
***
NS
NS
PDGF-BB (50 ng/mL): - - + + - - + +
Spermine(250 μM): - + - + - + - +
24 h
48 h
c)
PDGF-BB (50 ng/mL)
Control
Spermine
Control
Spermine
0 h
24 h
48 h
b)
Cell viability (%)
280
240
200
160
120
80
40
0
***
NS
***
***
NS
NS
PDGF-BB (50 ng/mL): - - + + - - + +
Spermine (250 μM): - + - + - + - +
24 h
48 h
d)
Cell migration (%)
100
80
60
40
20
0
***
***
***
***
NS
NS
PDGF-BB (50 ng/mL): - - + + - - + +
Spermine (250 μM): - + - + - + - +
24 h
48 h

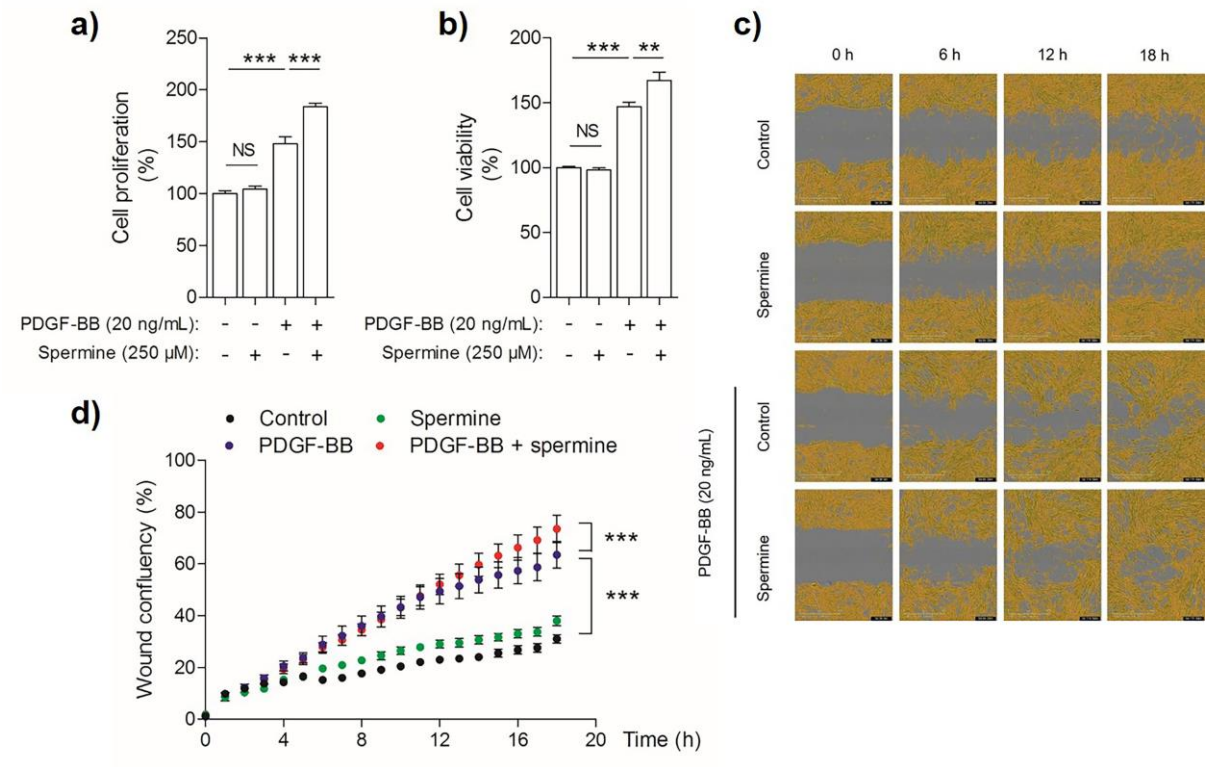
a)
Cell proliferation (%)
250
200
150
100
50
0
***
***
NS
PDGF-BB (20 ng/mL): - - + +
Spermine (250 µM): - + - +
b)
Cell viability (%)
200
150
100
50
0
***
**
NS
PDGF-BB (20 ng/mL): - - + +
Spermine (250 µM): - + - +
c)
0 h
6 h
12 h
18 h
Control
Spermine
Control
Spermine
PDGF-BB (20 ng/mL)
d)
Control
Spermine
PDGF-BB
PDGF-BB + spermine
Wound confluency (%)
100
80
60
40
20
0
0
4
8
12
16
20
Time (h)
***
***

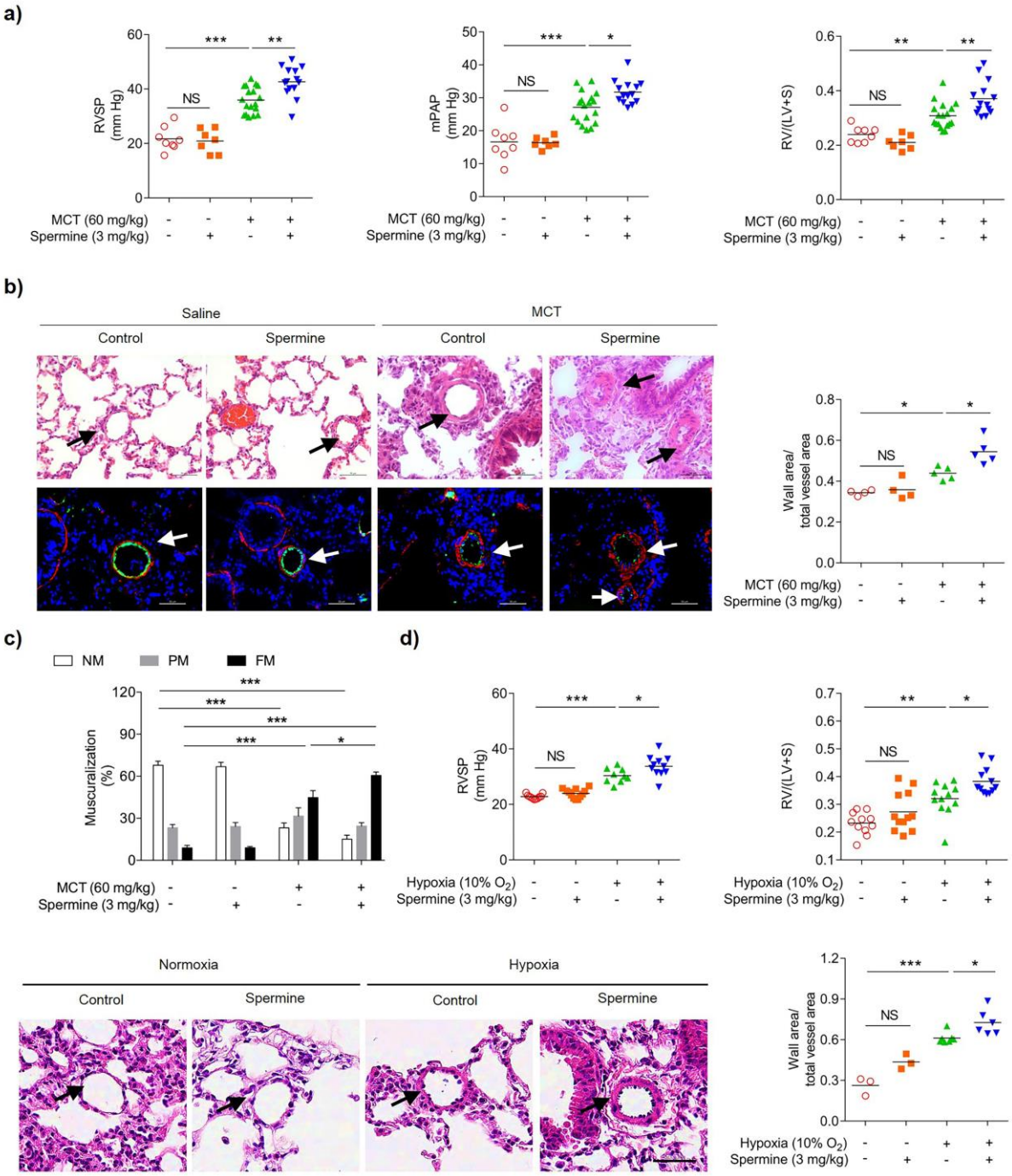
a)
RVSP (mm Hg)
mPAP (mm Hg)
RV/(LV+S)
NS
***
**
*
MCT (60 mg/kg)
Spermine (3 mg/kg)
b)
Saline
MCT
Control
Spermine
Wall area/ total vessel area
c)
NM
PM
FM
Muscularization (%)
d)
Hypoxia (10% O2)
Normoxia
Hypoxia

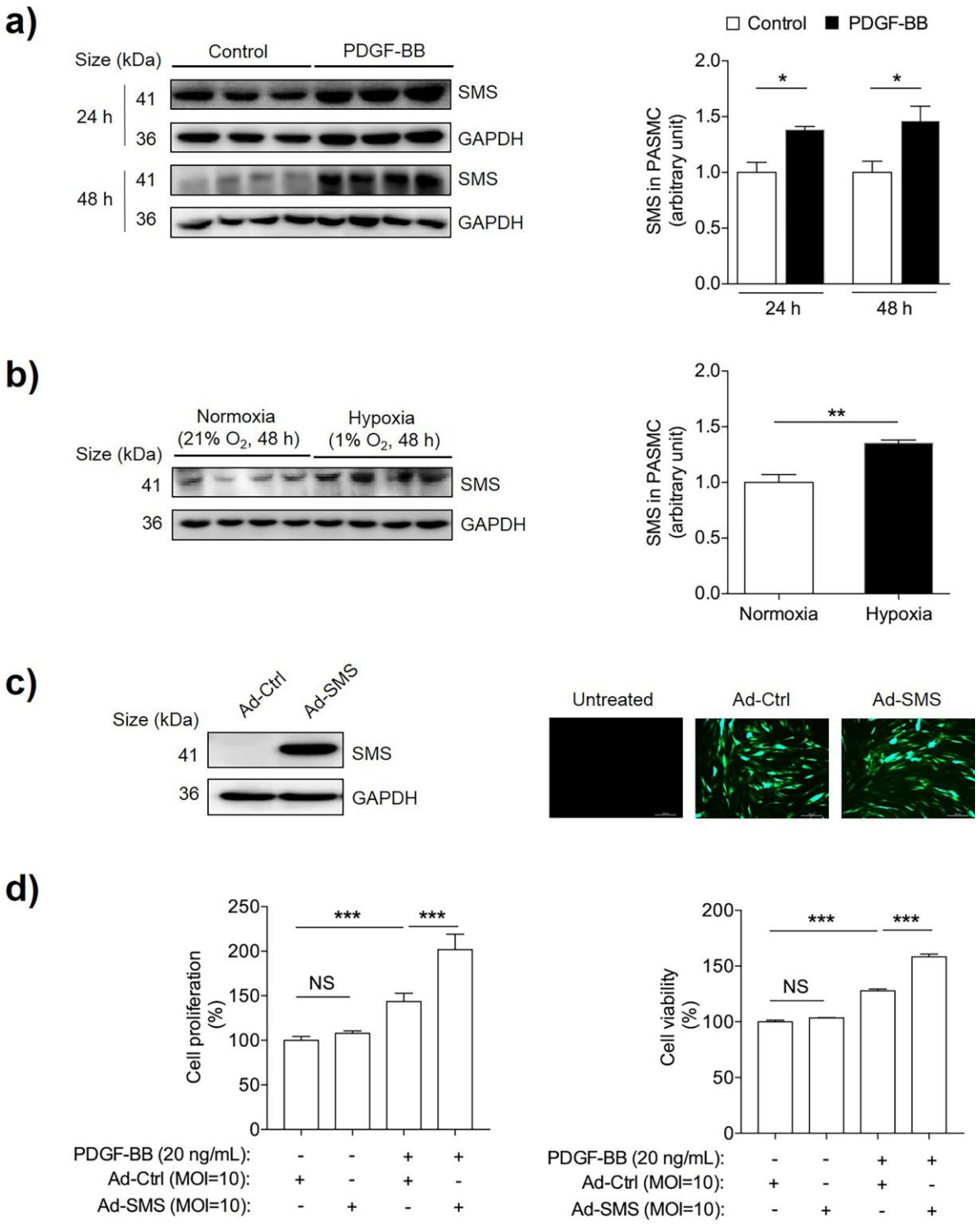
a)
Size (kDa)
Control
PDGF-BB
24 h
41
36
SMS
GAPDH
48 h
41
36
SMS
GAPDH
Control
PDGF-BB
SMS in PASMC (arbitrary unit)
2.0
1.5
1.0
0.5
0.0
*
*
24 h
48 h
b)
Normoxia (21% O2, 48 h)
Hypoxia (1% O2, 48 h)
Size (kDa)
41
36
SMS
GAPDH
SMS in PASMC (arbitrary unit)
2.0
1.5
1.0
0.5
0.0
**
Normoxia
Hypoxia
c)
Ad-Ctrl
Ad-SMS
Size (kDa)
41
36
SMS
GAPDH
Untreated
Ad-Ctrl
Ad-SMS
d)
Cell proliferation (%)
250
200
150
100
50
0
***
***
NS
PDGF-BB (20 ng/mL): - - + +
Ad-Ctrl (MOI=10): + - + -
Ad-SMS (MOI=10): - + - +
Cell viability (%)
200
150
100
50
0
***
***
NS
PDGF-BB (20 ng/mL): - - + +
Ad-Ctrl (MOI=10): + - + -
Ad-SMS (MOI=10): - + - +

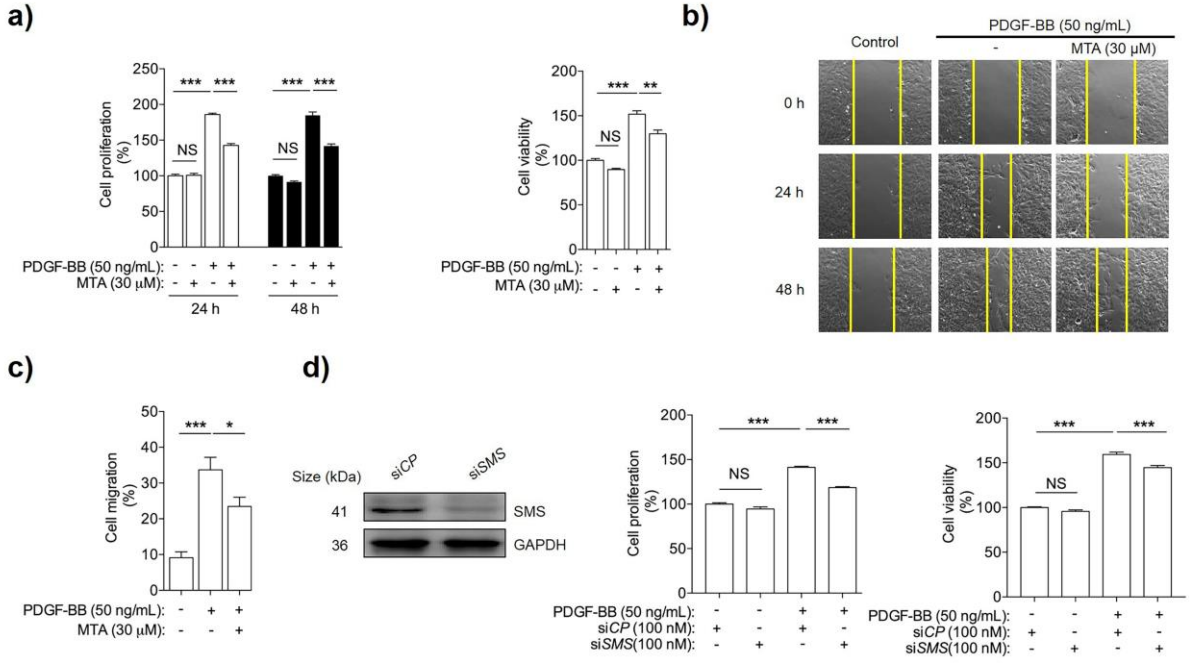
a)
Cell proliferation (%)
NS
***
PDGF-BB (50 ng/mL):
MTA (30 μM):
24 h
48 h
Cell viability (%)
**
b)
Control
PDGF-BB (50 ng/mL)
MTA (30 μM)
0 h
24 h
48 h
c)
Cell migration (%)
*
d)
Size (kDa)
siCP
siSMS
41
SMS
36
GAPDH
siCP (100 nM):
siSMS(100 nM):

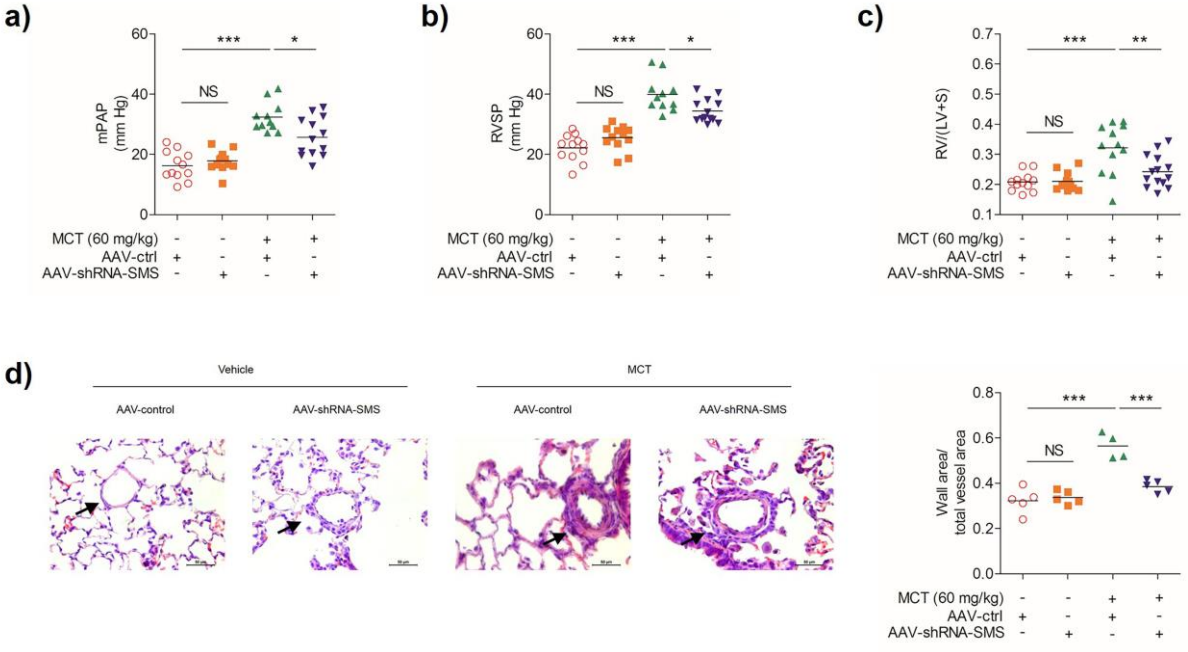
a)
mPAP (mm Hg)
60
40
20
0
***
*
NS
MCT (60 mg/kg) - - + +
AAV-ctrl + - + -
AAV-shRNA-SMS - + - +
b)
RVSP (mm Hg)
60
40
20
0
***
*
NS
MCT (60 mg/kg) - - + +
AAV-ctrl + - + -
AAV-shRNA-SMS - + - +
c)
RV/(LV+S)
0.7
0.6
0.5
0.4
0.3
0.2
0.1
***
**
NS
MCT (60 mg/kg) - - + +
AAV-ctrl + - + -
AAV-shRNA-SMS - + - +
d)
Vehicle
MCT
AAV-control
AAV-shRNA-SMS
AAV-control
AAV-shRNA-SMS
Wall area/ total vessel area
0.8
0.6
0.4
0.2
0.0
***
***
NS
MCT (60 mg/kg) - - + +
AAV-ctrl + - + -
AAV-shRNA-SMS - + - +

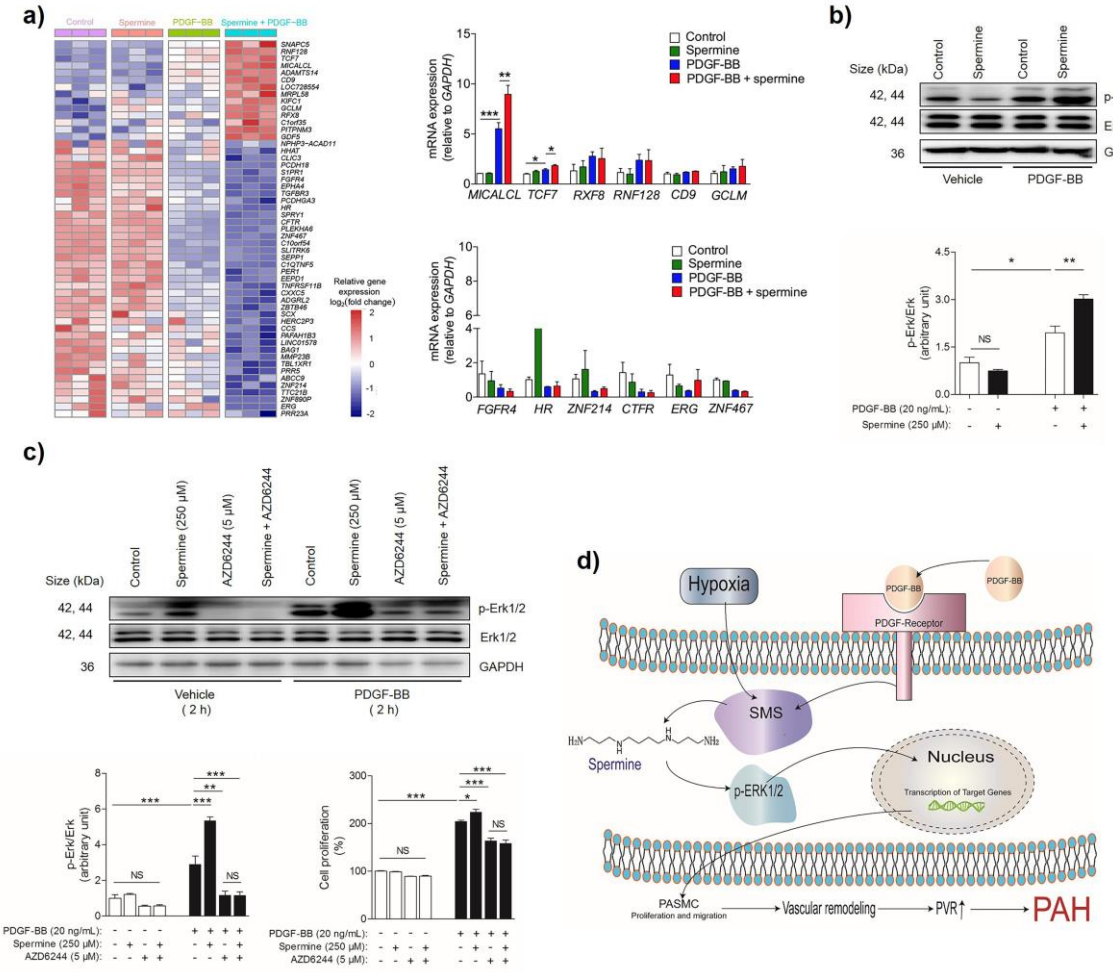
a)
Control
Spermine
PDGF-BB
Spermine + PDGF-BB
Relative gene expression log2(fold change)
mRNA expression (relative to GAPDH)
Control
Spermine
PDGF-BB
PDGF-BB + spermine
MICALCL TCF7 RXF8 RNF128 CD9 GCLM
FGFR4 HR ZNF214 CTFR ERG ZNF467
b)
Size (kDa)
Control
Spermine
Control
Spermine
42, 44
42, 44
36
p-Erk1/2
Erk1/2
GAPDH
Vehicle
PDGF-BB
p-Erk/Erk (arbitrary unit)
NS
PDGF-BB (20 ng/mL):
Spermine (250 μM):
c)
Size (kDa)
Control
Spermine (250 μM)
AZD6244 (5 μM)
Spermine + AZD6244
Control
Spermine (250 μM)
AZD6244 (5 μM)
Spermine + AZD6244
42, 44
42, 44
36
p-Erk1/2
Erk1/2
GAPDH
Vehicle (2 h)
PDGF-BB (2 h)
p-Erk/Erk (arbitrary unit)
Cell proliferation (%)
NS
PDGF-BB (20 ng/mL):
Spermine (250 μM):
AZD6244 (5 μM):
d)
Hypoxia
PDGF-BB
PDGF-BB
PDGF-Receptor
SMS
Spermine
p-ERK1/2
Nucleus
Transcription of Target Genes
PASMC
Proliferation and migration
Vascular remodeling
PVR↑
PAH

Supplementary Materials

Materials and Methods

Study subjects

Discovery cohort: Thirty patients were prospectively enrolled between April 2015 and September 2015 at FuWai Hospital, Chinese Academy of Medical Sciences and Peking Union Medical College (CAMS & PUMC). All patients were diagnosed with IPAH based on standard criteria from the recent guideline[1]. The exclusion criteria were as follows: (1) <18 or >70 years of age; (2) positive response to acute pulmonary vasodilator testing (administered via a right heart catheter), defined as a decrease in mean pulmonary arterial pressure (mPAP) from >10 to <40 mm Hg, and a preserved cardiac output; (3) major comorbidities, such as hypertension, hyperlipidemia, hepatitis B, or diabetes mellitus; (4) a family history of cancer, metabolic disease, or other severe heritable diseases. Thirty age- and sex-matched HCs were also recruited from FuWai Hospital.

Validation cohort*:* To verify whether spermine is elevated in the plasma of patients with IPAH, we prospectively enrolled another independent cohort of 45 patients with IPAH between June 2015 and January 2017 at FuWai Hospital. The same exclusion criteria were applied as described for the discovery cohort. Sixty age- and sex-matched HCs were recruited at either the Center of Health Examination of Peking University Hospital or FuWai Hospital.

Human blood samples

Blood samples were obtained from the cubital vein after the patients within one week from the time of right-heart catheterization documenting IPAH or HCs in the fasting state for approximately 12 h. None of the individuals had performed any exercise before blood collection. The blood was drawn into pre-cooled blood collection tubes containing EDTA and placed on ice. The tubes were centrifuged within 30 min at 4°C to separate the plasma from cells. The plasma was immediately frozen in liquid nitrogen and stored at −80°C until use to avoid potential degradation of the analytes.

Metabolomics

Metabolomic profiling was performed by LC-MS at the Institute of Materia Medica, CAMS & PUMC. This technique provided quantitative assessment of 74 metabolites covering the core network of energy, amino acid, amine, and nucleotide metabolisms, which were referenced to standard curves. The metabolites were identified based on mass and fragmentation analyses, and the full details of the methodology for the LC-MS conditions for the metabolites analyses were as described previously[2].

Plasma sample processing for metabolomics

A total of 100 μL plasma was transferred into a 1.5 mL Eppendorf tube, and then 20 μL reducing agent and 20 μL polar metabolite internal standards were added. The mixture was vortexed for 10 s, and then 400 μL acetonitrile was added to the tube. The sample was vortexed for 5 min and then centrifuged at 17,500 *g* for 10 min at 4°C. The protein precipitate was removed, and the solution was transferred to a glass tube.

The solution was dried in a nitrogen evaporator system at room temperature. The residue was redissolved with 100 μL acetonitrile/methanol (75:25, v/v) using an ultrasonic wave generator. The solution was transferred into another tube and then centrifuged at 17,500 *g* for 10 min at 4°C. The supernatant was applied to metabolite analysis by the Agilent 6490 Triple Quadrupole LC-MS method[2].

Rat pulmonary arterial smooth muscle cell isolation and culture

PASMCs were isolated from adult SD rats, as described by Rothman et al[3]. The cells were cultured and maintained in Dulbecco's modified Eagle (DMEM) medium/F12 (Gibco, New York, USA) containing 10% fetal bovine serum (FBS; Gibco) at 37°C with 5% CO_2. Smooth muscle cell identification was performed by immunofluorescence staining using a mouse polyclonal antibody against α-smooth muscle actin (#A2547; Sigma-Aldrich, Milwaukee, USA). In all experiments, the cells were cultured to 60%–70% confluence with no more than six passages.

siRNA transfection

PASMCs were transfected with SMS siRNA (si*SMS*) or a pooled siRNA control (si*CP*) using Lipofectamine 2000 (Thermo Fisher Scientific, Waltham, USA), according to the manufacturer's instructions. The PASMCs were cultured in DMEM/F12 with 10% FBS for 5 h after transfection and then applied to smooth muscle cell growth, migration, or protein assays. At 48 h after transfection, two of the SMS siRNA sequences (siRNA-1 and siRNA-2) were evaluated for knockdown efficiency of SMS

protein levels. siRNA-1 (5′-CCUUCAUACUUGGAAUUGUTT-3′) was the most effective.

Overexpression by adenovirus infection

Human PASMCs were infected with the pHBAd-MCMV-GFP adenovirus carrying cDNAs for green fluorescent protein (Ad-GFP) or human SMS (Ad-SMS). For virus infection, PASMCs were plated at approximately 50% confluency and infected at an MOI of 10 for 3 h at 37°C. The cells were then cultured for 36 h in DMEM/F12 without FBS. Cells were treated with PDGF-BB or the vehicle and subsequently applied to cell viability or proliferation assays.

Cell proliferation and viability assays

Pharmacological experiments*:* Rat or human PASMCs were seeded at 1×10^4 cells per well with complete medium in 96-well plates and incubated at 37°C with 5% CO_2 for 24 h. The cells were then serum starved in DMEM/F12 without FBS for another 24 h. Culture supernatants were discarded and replaced with DMEM/F12 without FBS, after which the cells were treated for 1 h with the vehicle (DMEM/F12 without FBS), spermine (#4264; Sigma-Aldrich), MTA (#D5011; Sigma-Aldrich), AZD6244 (#S1008; Selleck Chemicals, Houston, USA), or spermine combined with AZD6244. The cells were then exposed to recombinant rat PDGF-BB (#520-BB; R&D Systems, Minnesota, USA), recombinant human PDGF-BB (#220-BB-050; R&D Systems, Minnesota, USA) or the vehicle for 24 or 48 h. To assess cell proliferation, culture

supernatants were discarded, and cells were incubated with 0.1% crystal violet for 10 min at room temperature. The cells were washed three times, and 100 μL of 1% SDS was added to each well. The plates were gently shaken to dissolve the dye thoroughly in an enzyme-linked immunosorbent detector for 10 min at room temperature. Optical density (OD) was determined at 570 nm using a microplate reader (Infinite M200 Pro; Tecan, Switzerland). 5-bromo-2'-deoxyuridine (BrdU) incorporation assays (QIA58, Calbiochem, San Diego, CA) were performed in a 96-well plate according to manufacturer's instructions to validate the proliferative effect of spermine in PASMCs. To assess cell viability, culture supernatants were discarded and replaced with CCK-8 solution (Dojindo Molecular Technologies Inc, Kumamoto, Japan), and cells were incubated at 37°C with 5% CO_2 for 1.5 h. OD was then determined at 450 nm.

siRNA transfection experiments*:* Rat PASMCs were transfected with si*SMS* or si*CP*, cultured for 24 h in complete medium, serum starved for 24 h, and then treated with PDGF-BB or the vehicle. Cell proliferation and viability were assessed by crystal violet and CCK-8 assays, respectively, as described above.

Adenovirus infection experiments: Human PASMCs were infected with Ad-SMS or Ad-GFP and then cultured for 3 h in DMEM/F12 with 10% FBS. After serum starvation for 24 h, cells were treated with recombinant human PDGF-BB (220-BB; R&D System) or the vehicle. Cell viability and proliferation assays were performed as described above.

Cell migration

Wound healing assay: Rat PASMCs were seeded at 1×10^5 cells per well with DMEM/F12 medium containing 10% FBS in 6-well plates to form a monolayer. Cells were washed three times with phosphate-buffered saline (PBS) prior to addition of DMEM/F12 without FBS. At 24 h after serum starvation, the monolayer was scratched with a P200 pipette tip, and the cells were washed twice with PBS before adding the vehicle (DMEM/F12 without FBS), PDGF-BB, spermine (250 μM) plus PDGF-BB, or MTA (30 μM) plus PDGF-BB. Phase contrast images were obtained at ×100 magnification at 0, 24, and 48 h after scratching. Images of each individual scratch were obtained, and cell migration rates were calculated using Image-Pro Plus 6.0 analysis software (Media Cybernetics, Bethesda, USA), as described previously[4].

Transwell assay: Rat PASMCs were transfected with si*SMS* or si*CP* and cultured for 24 h in complete medium. They were serum starved for 24 h and then digested, washed twice with PBS, and resuspended in serum-free DMEM/F12. Cell density was adjusted to 5×10^4 cells/mL. The experiment was performed in 24-well 8-μm Transwell plates (Corning-Costar, Corning, New York, USA) with three chambers per group and 100 μL cell suspension per chamber. The lower chambers contained 600 μL DMEM/F12 in the presence or absence of PDGF-BB. Cells were incubated at 37°C with 5% CO_2. After 18 h, the cells were fixed with 4% paraformaldehyde for 30 min at room temperature, followed by a 0.1% crystal violet dye solution for 5 min and washed twice. The number of stained cells was counted in randomly selected fields under an inverted microscope. Three independent experiments were performed.

Automated wound healing assay: Human PASMC migration was evaluated by a

wound healing assay using an IncuCyte ZOOM imaging system (Essen Bioscience, Ann Arbor, USA), as described previously[5]. Briefly, cells were seeded in 96-well plates at 1.5×10^4 cells per well. After 24 h of serum starvation, the monolayers were scratched with a 96-Well Wound Maker apparatus (Essen Bioscience) to generate an approximately 600 μm-wide wound. To remove debris, cells were washed twice with PBS prior to administration of the vehicle (DMEM/F12 without FBS), spermine (250 μM), PDGF-BB, or spermine (250 μM) plus PDGF-BB. The wound healing assay was then conducted with the IncuCyte ZOOM imaging system (Essen Bioscience) that automatically and continuously acquires and analyzes images using bright field microscopy, providing informative and real-time kinetic data. Cell migration rates are reported as the relative wound density (RWD) calculated by an algorithm measuring cell density in the wound area relative to the cell density outside of the wound area at intervals of 1 h. Representative images were obtained at ×100 magnification at 0, 6, 12, and 18 h post-scratching.

Animal experimental design

Male SD rats (~8 weeks; Charles River Laboratories China) injected with MCT (#C2401; Sigma-Aldrich) and male C57BL/6 mice (~8 weeks; Charles River Inc.) exposed to chronic hypoxia were used in this study. All procedures involving rats were performed in accordance with the Guidelines for Animal Experimentation established and approved by the Animal Care and Use Committee of FuWai Hospital. All experiments involving mice were approved by the Ethics and Animal Care Committee

of the University of Illinois at Chicago. All animal experiments conformed to the Guide for the Care and Use of Laboratory Animals (NIH publication no. 85-23, revised 1996).

To investigate the effects of spermine (#85590; Sigma-Aldrich) on the development of pulmonary hypertension, adult male SD rats (220–240 g) were purchased from Charles River (Beijing, China) and allowed to acclimate for 5 days in a specific pathogen-free grade barrier system with alternating 12 h light/dark cycles at a relative humidity of 50%±5% and 25°C. They were administered a single subcutaneous injection of 60 mg/kg MCT or sterile saline (vehicle control). To optimize the dose of spermine, two independent experiments were conducted. In the first experiment, rats received daily intraperitoneal injections of spermine (20 mg/kg) or a similar volume of saline as the vehicle for 7 days (n = 12 per group). In the second experiment, rats received daily intraperitoneal injections of spermine (10 mg/kg) beginning on Day 14 after MCT administration and continuing for another 6 days (n = 4–5 per group). Eventually, spermine was injected intraperitoneally once daily at a dose of 1 or 3 mg/kg body weight from Day 14. On Day 21, hemodynamics and RVHI were assessed as described in our previous study[6], and lung tissues were harvested and stored in liquid nitrogen or formalin for subsequent analysis.

To examine the effects of spermine on the development of hypoxia-induced pulmonary hypertension, we established a pulmonary hypertension mouse model using healthy adult male C57BL/6 mice. The mice were placed in a hypoxic chamber containing 10% O_2 after acclimatization for 5 days, as described above. After exposure

to hypoxia for 2 weeks, spermine was injected intraperitoneally at a dose of 3 mg/kg body weight once daily. At Day 28, hemodynamics and RVHI were assessed, and then lung tissues were harvested and stored immediately at −80°C or in formalin for subsequent analysis.

To investigate the effect of SMS silencing on the pathogenesis of PAH, SD rats were anesthetized by an intraperitoneal injection of ketamine hydrochloride (100 mg/kg), placed in the supine position at a 45° angle, and then administered a 100 μL solution containing either 1.3×10^{10} viral particles of AAV-shRNA-SMS or the control (AAV-ctrl). Two weeks later, the rats were randomized and administered with MCT or sterile saline for another 3 weeks. At Day 35, hemodynamics and RVHI were assessed as described above. Lung tissues were fixed in formalin or stored at −80°C.

To investigate the effect of SMS overexpression on the pathogenesis of PAH, healthy adult male C57BL/6 mice were anesthetized by using an i.p. injection of ketamine (100 mg/kg) and xylazine (10 mg/kg), and then mice were delivered intratracheally with 2×10^{11} GC of either AAV-SMS or AAV-null in a final solution of 100 μL, the mouse was maintained at a 45° angle for 1 min. Two weeks later mice were then transferred a hypoxia chamber (10% O_2) or in normoxia for the additional two weeks. Hemodynamics and right heart hypertrophy were assessed as described above.

Histopathology

Lungs were properly inflated with 0.9% saline before 10% formaldehyde fixation for

48 h. Pulmonary artery remodeling was assessed using Image-Pro Plus 6.0 software after the lungs were stained with hematoxylin and eosin. Vessel remodeling was calculated as (the external vessel area – the internal vessel area)/the external vessel area, as described previously[7].

Immunofluorescence staining of rat lung tissues was performed to assess pulmonary arteriolar muscularization. A rabbit polyclonal anti-von Willebrand factor antibody (#ab6994; Abcam), followed by an Alexa-488-conjugated anti-rabbit secondary antibody (#4412; CST) were used to visualize endothelial cells. A mouse monoclonal anti-smooth muscle-l actin antibody (#A2547; Sigma-Aldrich), followed by Alexa-594-conjugated anti-mouse secondary antibody (#8890; CST) were used to visualize PASMCs. Images were acquired at ×200 magnification to assess the degree of pulmonary arteriolar muscularization in a single blind fashion. A total of 60–80 intra-acinar vessels accompanying either alveolar ducts or alveoli were evaluated per rat. Each vessel was categorized as nonmuscularized (no apparent muscle), partially muscularized (only a crescent of muscle), or fully muscularized (complete medial coat of muscle). The percentages of nonmuscularized and partially or fully muscularized vessels were calculated by dividing the number of vessels in each category by the total number of blood vessels counted per section.

Western blot analysis

SMS and OPN expression and activation levels of intracellular signaling molecules in cells from various groups were detected and quantified by western blot analyses. A

total of 20 μg protein extract was resolved by 8%, 12%, or 15% SDS-polyacrylamide gel electrophoresis, transferred onto a polyvinylidene fluoride membrane, and blocked with 5% BSA in Tris-buffered saline (TBS) for 1 h at room temperature. The membrane was then washed three times in TBS with 0.1% Tween 20 (TBS-T) and incubated overnight at 4°C with anti-SMS (#ab156879; Abcam), anti-OPN (#ab8448; Abcam), anti-phosphorylated Erk1/2 (p-Erk1/2) (#4695; CST), anti-phosphorylated AKT (p-AKT) (#4060; CST), anti-phosphorylated MLC (p-MLC) (#3671; CST), or anti-phosphorylated smad2 (p-smad2) (#3101; CST) antibodies. The membranes were washed three times in TBS-T for 10 min each wash and then incubated with anti-rabbit or anti-mouse IgG conjugated with horseradish peroxidase in TBS. After another three washes with TBS-T for 10 min each wash, the membranes were reacted with a chemiluminescence system for 1 min and then exposed to X-ray film. As a loading control, all blots were reprobed with an anti-glyceraldehyde-3-phosphate dehydrogenase (GAPDH) monoclonal antibody (#5174; CST). Protein expression levels were quantified by scanning densitometry using the Quantity One 1-D analysis system.

RNA-seq analysis

Total RNA in human PASMCs was isolated and applied to RNA-seq analysis. Construction and sequencing of the cDNA library were performed at the Beijing Genomics Institute using the BGISEQ-500 platform. High quality reads were aligned to the human reference genome (GRCh38) using Bowtie2. Expression levels of each

detected gene were normalized to FPKM (fragments per kilobase of exon model per million mapped reads) using RNA-seq by expectation maximization.

Real-time PCR

Total RNA was isolated and then reverse transcribed into cDNA using a SuperScript® III First-Strand Synthesis Kit (#18080-051; Thermo Fisher Scientific), according to the manufacturer's instructions. FastStart Universal SYBR Green Master (#04913850001; Roche, Basel, Switzerland) was used to quantify the PCR amplification products. Relative mRNA expression levels of target genes were normalized to GAPDH expression and calculated using the $2^{(-\Delta\Delta CT)}$ method. Primer pairs are listed in **Supplementary Table S4**.

Statistical analysis

MetaboAnalyst 3.0 software was used to explore potentially significant metabolites and meaningful pathways involved in the pathophysiology of PAH. Metabolites with a *P*-value of <0.05 and fold change of >2.0 or <0.5 were considered as significant. Univariate analysis methods were used to provide a preliminary overview of the features potentially significant to distinguish patients with IPAH from HCs. For further exploratory data analysis, PLS-DA was used to visually distinguish between groups. Metabolomic data were mean centered and auto scaled to reduce noise before data processing. The variable importance in the projection (VIP) value of each variable in the model was calculated to indicate its contribution to the classification. A

higher VIP value represented a stronger contribution to discrimination among groups. The quality and predictability of the PLS-DA model were evaluated using R2Y (cum) and Q2 (cum) values, respectively. To assess the significance of class distinction, a permutation test was performed. Pathway analysis combined results from pathway enrichment analysis with those of pathway topology analysis to identify the most relevant pathways involved.

Data are presented as the mean ± standard error of the mean (s.e.m.) or median (IQR). Comparisons between two groups were performed using the Student's t-test if data were distributed normally. Otherwise, the Mann–Whitney U test was used. Comparisons of more than three groups were performed by analysis of variance (ANOVA) and Tukey's post-hoc test with GraphPad Prism version 5.0 or the Kruskal–Wallis test, as appropriate. *P*-values of <0.05 were considered as statistically significant.

Supplementary Figures and legends

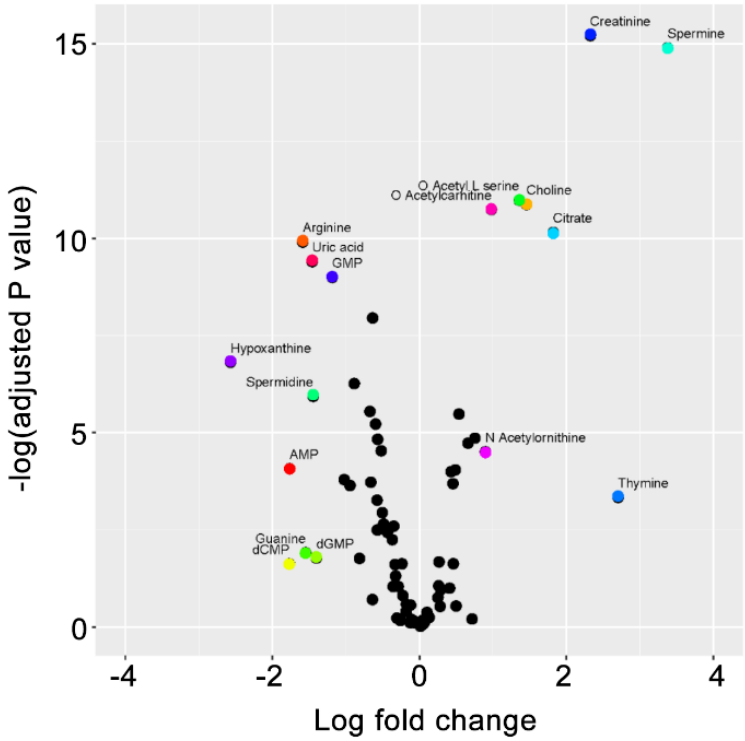

Supplementary Figure S1 Volcano plots of metabolites in the plasma of healthy controls (HCs) and patients with idiopathic pulmonary arterial hypertension (IPAH). The plots showed 8 upregulated metabolites (right) and 9 downregulated metabolites (left) in the IPAH cohort compared to the matched HCs. Each plot represents a metabolite. Differentiating metabolites with a fold change of >2.0 or <0.5 and *P*-value

of <0.05 are highlighted.

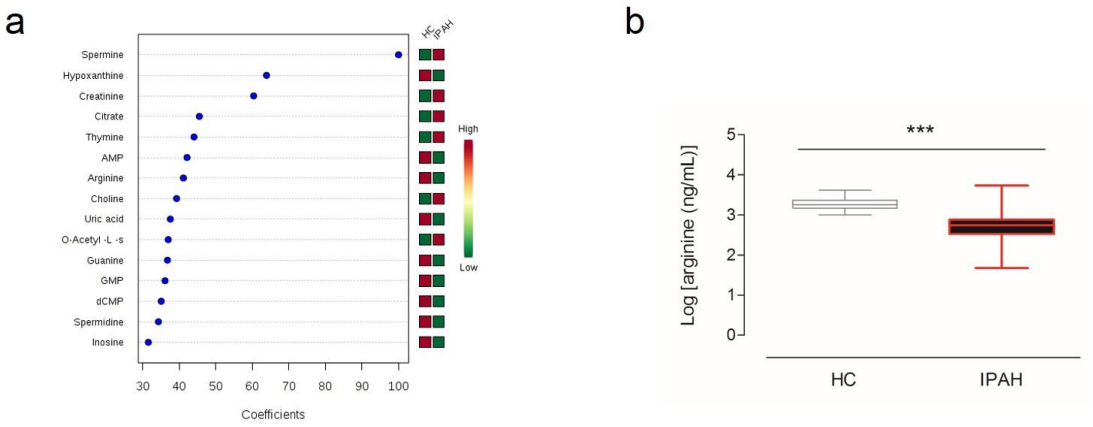

Supplementary Figure S2 Ranking of differentiating metabolites and comparison of arginine in the plasma of healthy controls (HCs) and patients with idiopathic pulmonary arterial hypertension (IPAH). (**a**) Ranking of differentiating metabolites was based on a weighted sum of partial least squares (PLS) regression coefficients. (**b**) Arginine (after base 10 log transformation) in the plasma of HCs and patients with IPAH in the discovery cohort was detected by liquid chromatography-mass spectrometry (LC-MS). Arginine levels were lower in IPAH patients than in HCs (n = 30 per group). ***P < 0.001; Mann–Whitney U test. Data are presented as box-and-whisker plots.

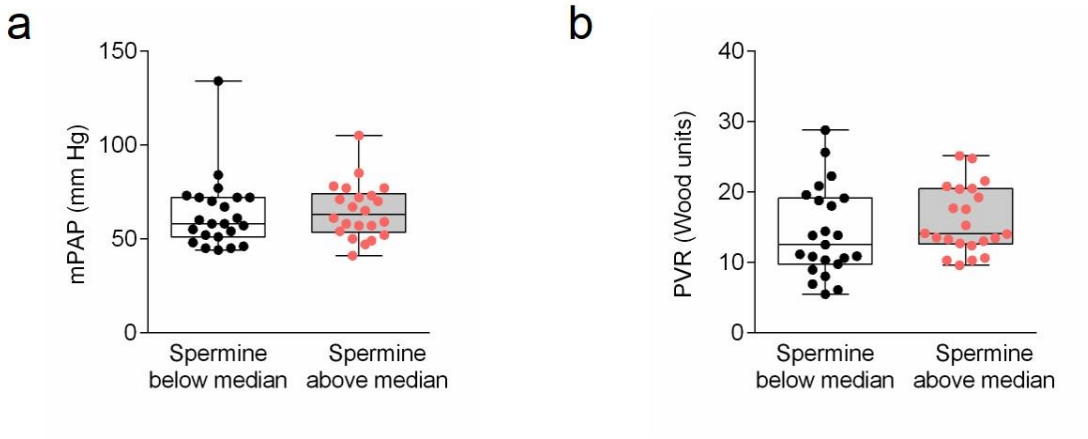

Supplementary Figure S3 Hemodynamic parameters, including pulmonary arterial pressure (**a**) and pulmonary vascular resistance (**b**), exhibited no significant differences between high (n = 22) and low (n = 23) spermine groups divided by the median value.

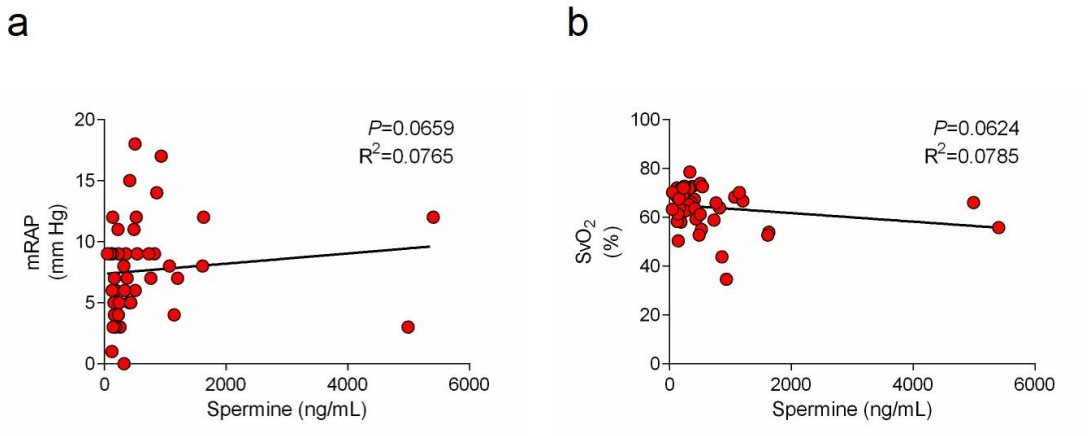

Supplementary Figure S4 Correlation of plasma spermine and hemodynamic parameters mean right atrial pressure (mRAP), and mixed venous oxygen saturation (SvO_2) in patients with IPAH (n=45) were depicted in scatter plot, respectively. Data were analyzed by Spearman's correlation.

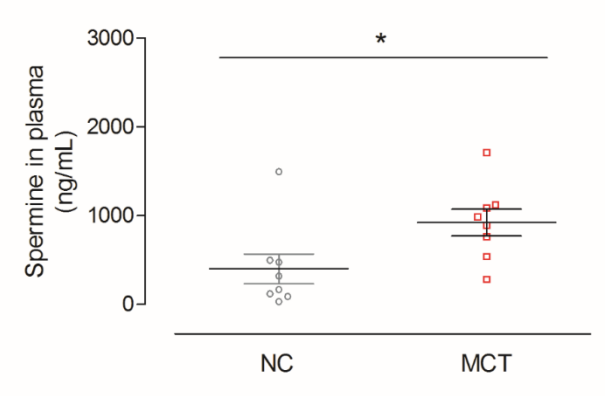

Supplementary Figure S5 Concentrations of spermine in the plasma of the experimental pulmonary hypertension animal model after monocrotaline (MCT) administration (n = 8 per group). NC = normal control. *P < 0.05; Student's t-test. Data are the mean ± s.e.m.

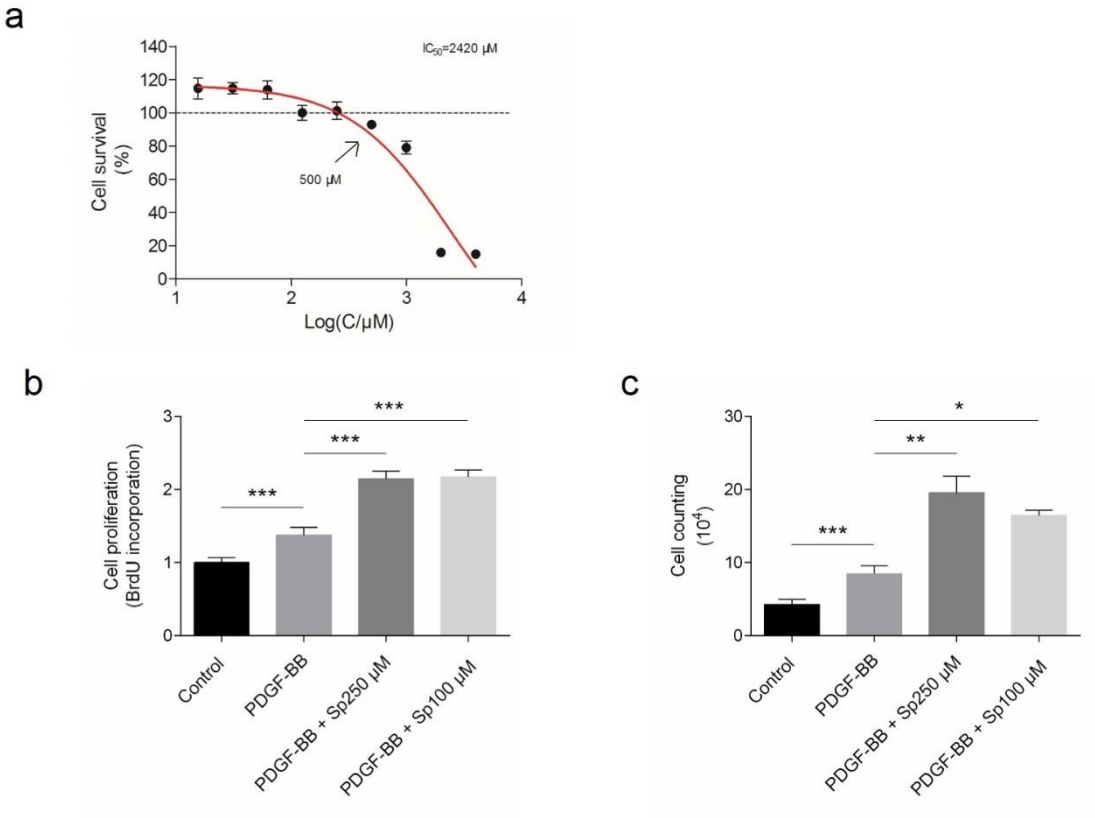

Supplementary Figure S6 Effects of spermine on proliferation of pulmonary arterial smooth muscle cells (PASMCs). (**a**) different concentrations of spermine on the survival of PASMCs (n = 6 per group). (**b**) PASMC proliferation used by BrdU assay (n = 4 for per group). (**d**) cell proliferation used by cell counting (n = 4 for per group). *P < 0.05, **P < 0.01, ***P < 0.001; one-way ANOVA, Tukey's post-hoc test. Data represent mean ± s.e.m.

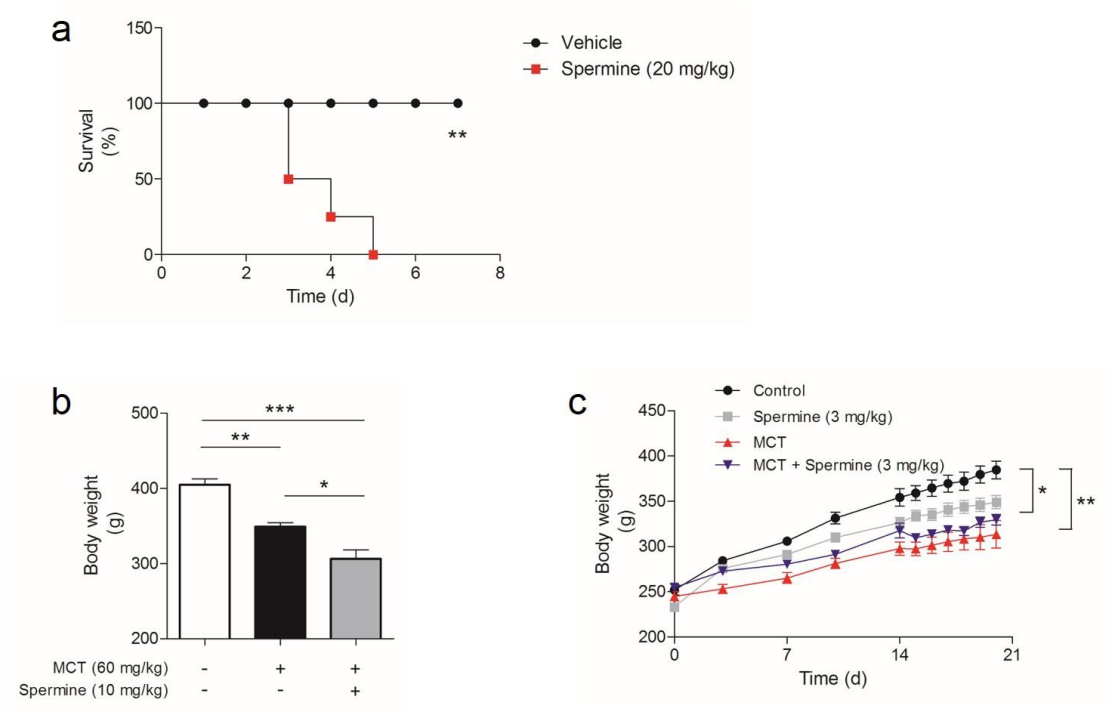

Supplementary Figure S7 Effects of spermine at various doses on survival and body weight of rats. (**a**) Survival curve demonstrating a markedly lower survival rate in rats that received daily intraperitoneal injections of spermine (20 mg/kg) compared with rats without spermine treatment (n = 12 per group). $^{**}P < 0.01$; log-rank (Mantel–Cox) test. (**b**) Body weight of rats that received daily intraperitoneal injections of spermine (10 mg/kg) beginning on Day 14 after monocrotaline (MCT) administration and continuing for another 6 days, demonstrating greater loss of weight compared with rats without spermine treatment after MCT administration (n = 4 for control group, n = 5 for all other groups). $^{*}P < 0.05$, $^{**}P < 0.01$, $^{***}P < 0.001$; one-way ANOVA, Tukey's post-hoc test. Data are the mean ± s.e.m. (**c**) Body weights of rats that received daily intraperitoneal injections of spermine (3 mg/kg) beginning on Day 14 after MCT administration and continuing for another 6 days, demonstrating no significant weight loss compared with rats without spermine treatment after MCT

administration (n = 8 for control group, n = 7 for spermine group, n = 10 for MCT group, and n = 7 for MCT + spermine group). *P < 0.05, **P < 0.01; one-way ANOVA, Tukey's multiple comparison test. Data are the mean ± s.e.m.

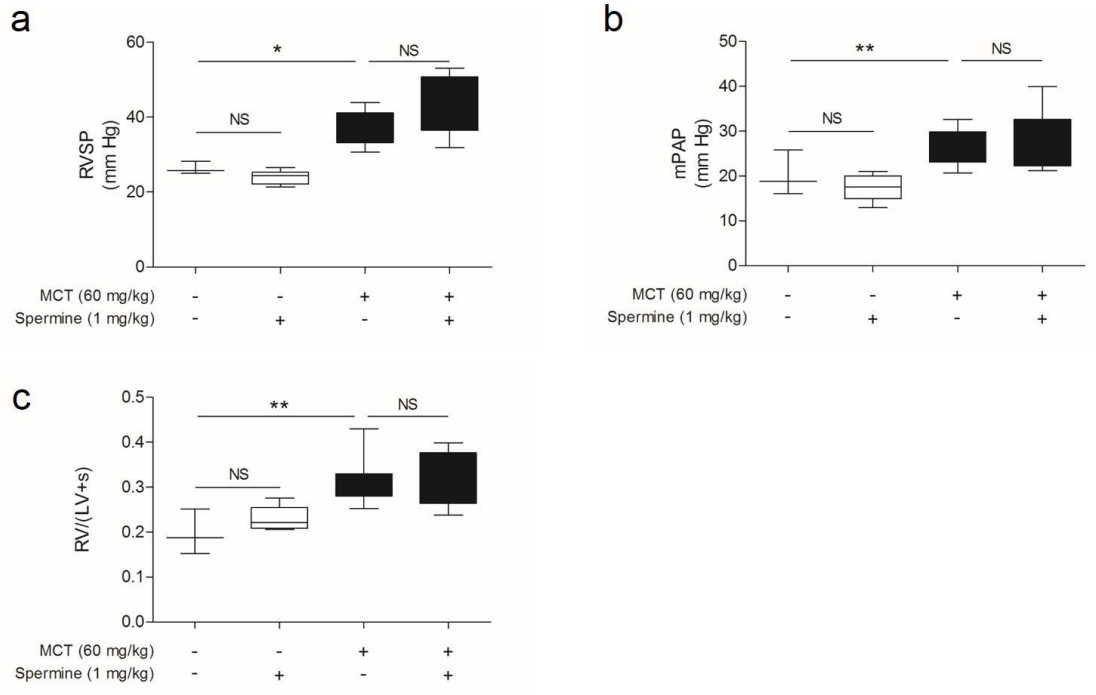

Supplementary Figure S8 Effects of spermine (1 mg/kg) in the pulmonary hypertension rodent model after monocrotaline (MCT) administration. (**a**) Assessment of right ventricular systolic pressures (RVSP) in control rats (n = 3), spermine-treated rats (n = 8), MCT-induced PH rats (n = 8), and MCT + spermine-treated rats (n = 7). (**b**) Mean pulmonary arterial pressure (mPAP) of the same animals in **a**. **(c)** Right ventricular hypertrophy index (RVHI) of the same animals in **a**. *P < 0.05, **P < 0.01; one-way ANOVA, Tukey's post-hoc test. Data are the mean ± s.e.m.

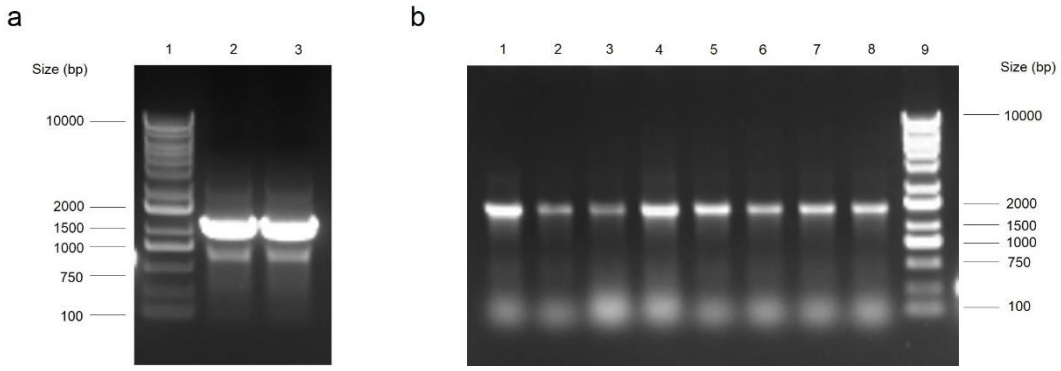

Supplementary Figure S9 Construction of the recombinant human spermine synthase (SMS) gene adenoviral vector. (**a**) Purification of the PCR product for the *SMS* gene by 1% agarose gel electrophoresis. Lane 1: DNA marker; lanes 2 and 3: *SMS* PCR products. (**b**) PCR amplification analysis of monoclonal colonies. Lanes 1–8: monoclonal identification; lane 9: DNA marker.

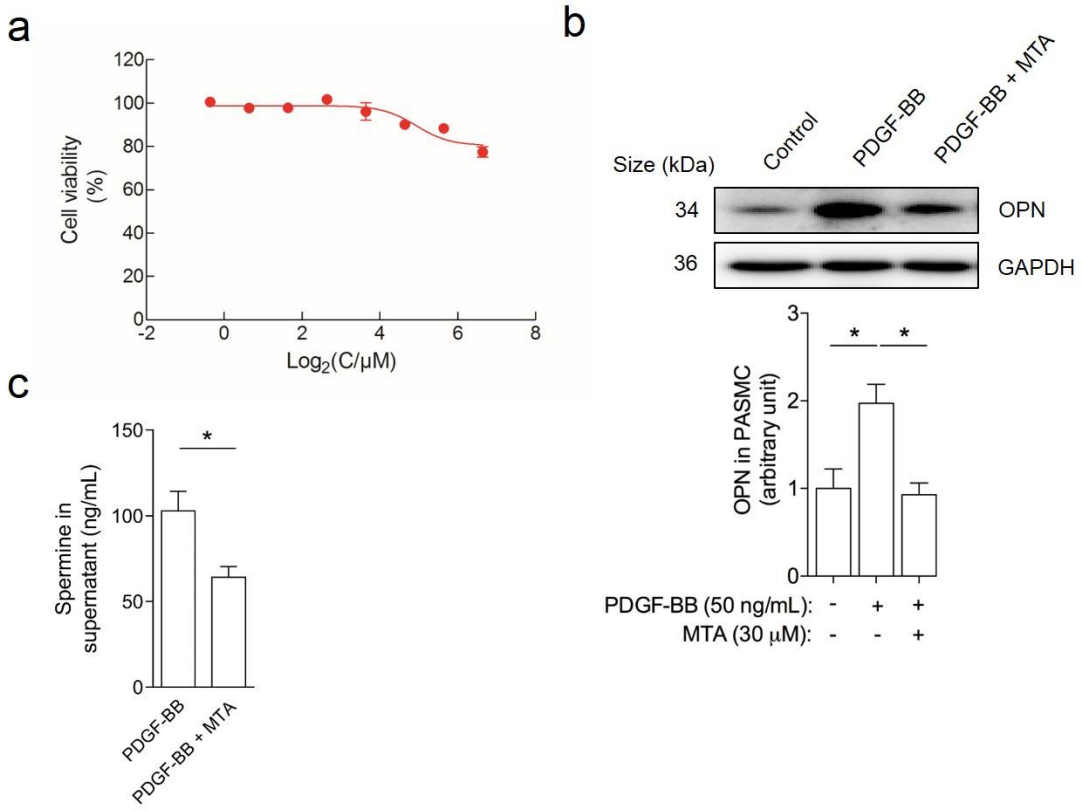

Supplementary Figure S10 (**a**) Effects of different concentrations of spermine synthase inhibitor 5′-deoxy-5′-methylthioadenosine (MTA) on the viability of rat pulmonary arterial smooth muscle cells (PASMCs). MTA at 50 μM or below did not affect the viability of PASMCs and exhibited no toxic effects (n = 4 per group). (**b**) Quantification of osteopontin (OPN) expression by western blotting in rat PASMCs treated with platelet-derived growth factor-BB (PDGF-BB) in the presence or absence of MTA (n = 3 per group). *P < 0.05; one-way ANOVA, Tukey's post-hoc test. Data are the mean ± s.e.m. (**c**) Effects of 30 μM MTA on spermine secretion into the culture supernatant of rat PASMCs (n = 5 per group). *P < 0.05; Student's t-test. Data are the mean ± s.e.m.

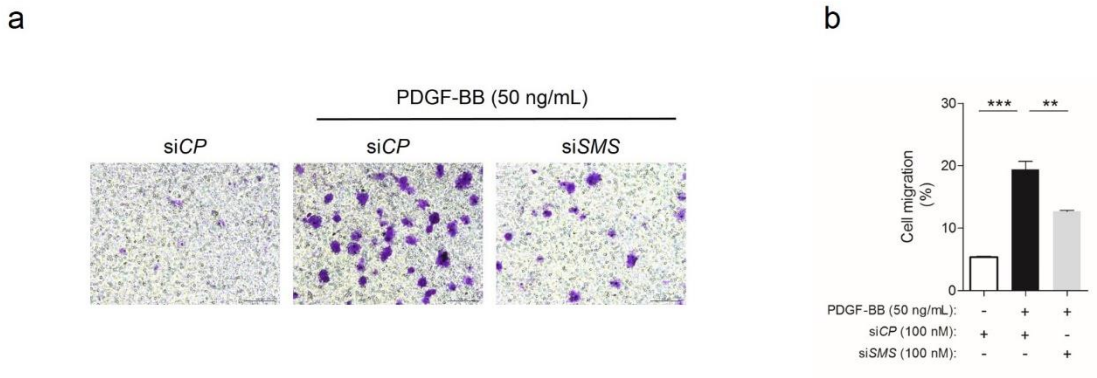

Supplementary Figure S11 Effects of spermine synthase (SMS) inactivation on the migration of human pulmonary arterial smooth muscle cells (PASMCs) stimulated by platelet-derived growth factor-BB (PDGF-BB). (**a**) Representative images of rat PASMC migration after PDGF-BB stimulation for 18 h following scrambled siRNA (si*CP*) or SMS-specific siRNA (si*SMS*) transfection for 48 h using the transwell assay. Scale bar, 100 μm. (**b**) In response to PDGF-BB, SMS inactivation led to decreased migration compared with PASMCs transfected with si*CP* (n = 3 per group). $^{**}P < 0.01$, $^{***}P < 0.001$; one-way ANOVA, Tukey's post-hoc test. Data are the mean ± s.e.m.

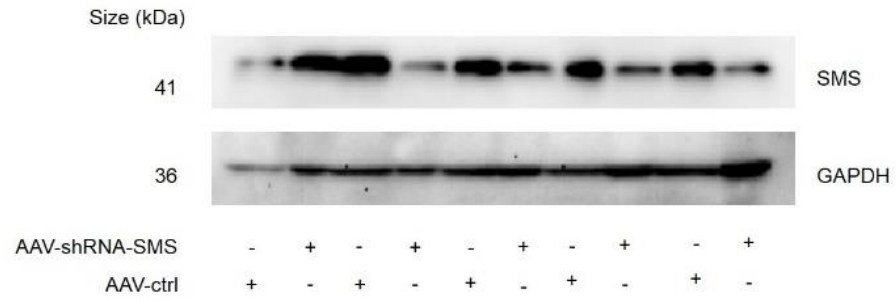

Supplementary Figure S12 Effects of gene silencing on rat lung tissues after exposure to a recombinant adeno-associated virus 6 carrying spermine synthase short hairpin RNA (AAV-shRNA-SMS) or control adeno-associated virus (AAV-ctrl) for 5 weeks, as identified by western blotting.

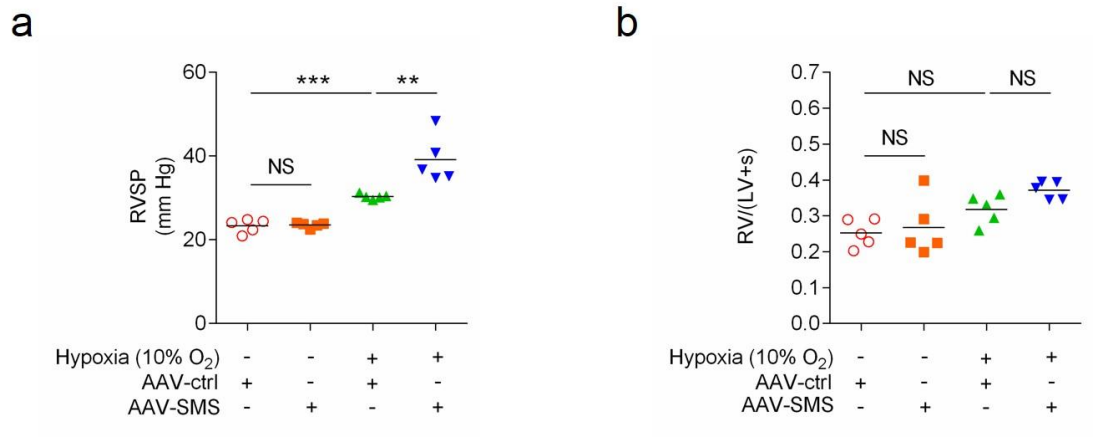

Supplementary Figure S13 Effects of overexpressing spermine synthase (SMS) on hypoxia-induced pulmonary hypertension in mice. (**a**) right ventricular systolic pressure (RVSP), (**b**) right ventricular hypertrophy index (RVHI). $n = 5$ for per group. *$P < 0.05$, **$P < 0.01$; one-way ANOVA, Tukey's post-hoc test. Data are the mean ± s.e.m.

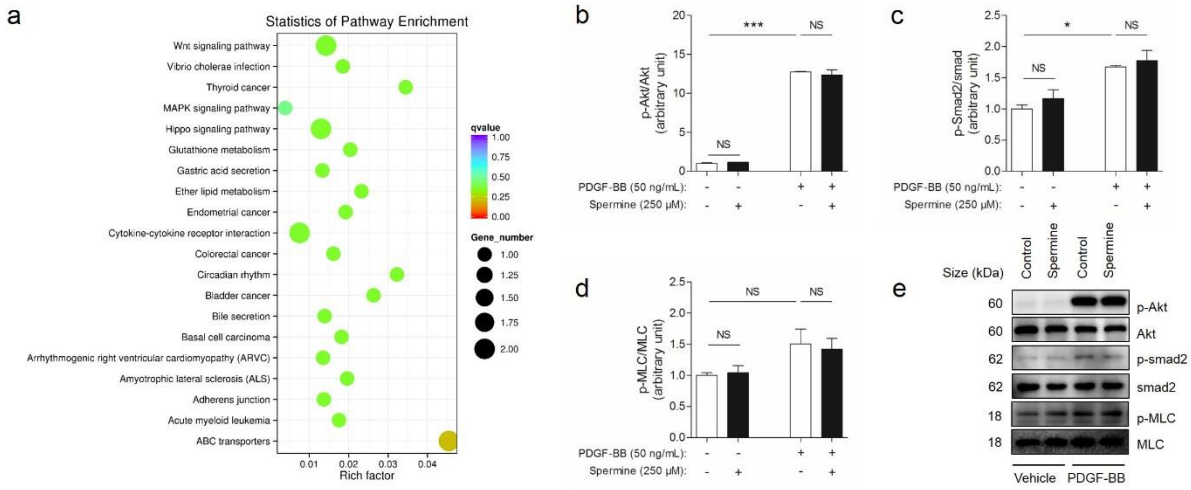

Supplementary Figure S14 KEGG pathway analysis and phosphorylation of candidate signaling pathways in response to PDGF-BB in the presence or absence of spermine. (**a**) Bubble chart displayed statistics of pathway enrichment of differentially expressed genes in response to PDGF-BB with spermine compared with those treated with PDGF-BB alone. Scanning densitometry using Quantity One 1-D to quantify p-Akt (**b**), p-Smad2 (**c**), and p-MLC (**d**) expression in rat pulmonary arterial smooth muscle cells (PASMCs), normalized to total Akt (n = 3 per group), Smad2 (n = 3 per group), and MLC (n = 4 per group), respectively. (**e**) Effects of spermine on p-Akt, p-Smad2, and p-MLC expression in PASMCs in the presence or absence of platelet-derived growth factor-BB (PDGF-BB), as assessed by western blotting. *P < 0.05, ***P < 0.001; one-way ANOVA, Tukey's post-hoc test. Data are the mean ± s.e.m.

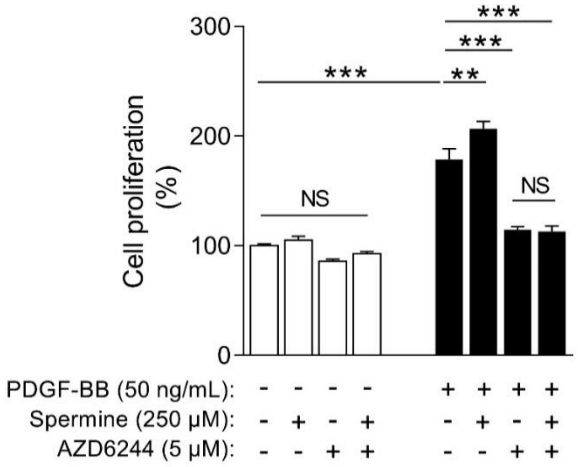

Supplementary Figure S15 Erk1/2 phosphorylation inhibitor AZD6244 suppresses spermine-induced proliferation of rat pulmonary arterial smooth muscle cells (PASMCs) in response to platelet-derived growth factor-BB (PDGF-BB). Effects of spermine on the proliferation of rat PASMCs in the presence or absence of AZD6244 (5 μM) after PDGF-BB (50 ng/mL) stimulation for 48 h (n = 5 per group). ***P* < 0.01, ****P* < 0.001; one-way ANOVA, Tukey's post-hoc test. Data are the mean ± s.e.m.

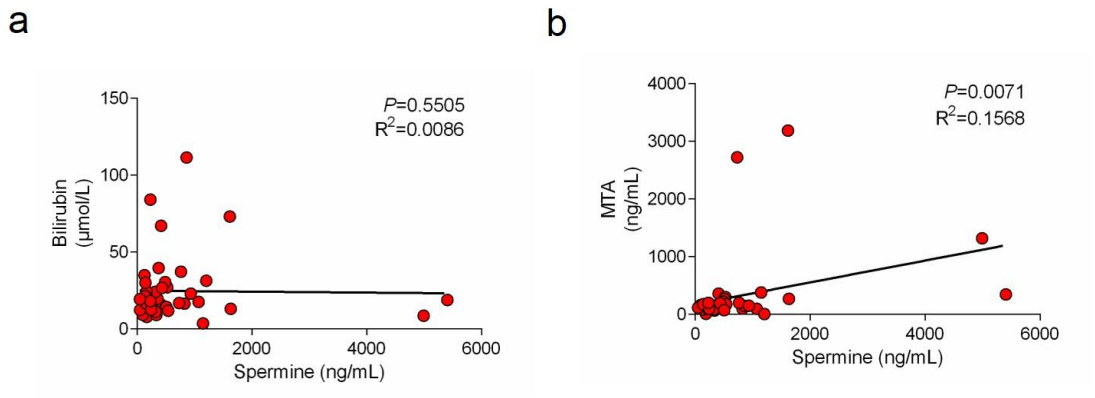

Supplementary Figure S16 Correlations of plasma spermine and bilirubin, and MTA in patients with IPAH (n=45) were depicted in scatter plot, respectively. Data were analyzed by Spearman's correlation.

Supplementary Table S1 Cohort characteristics

	Discovery cohort		**Validation cohort**	
	Healthy controls (*n* = 30)	IPAH patients (*n* = 30)	Healthy controls (*n* = 60)	IPAH patients (*n* = 45)
Age (years)	34.1 ± 11.5	30.4 ± 9.4	28.9 ± 6.6	31.8 ± 7.0
Female, n (%)	22 (73)	25 (83)	52 (87)	39 (87)
BMI (kg/m^2)	-	21.3 ± 2.3	-	22.5 ± 3.2
PAWP (mm Hg)	-	9.2 ± 3.0	-	9.0 ± 2
mPAP (mm Hg)	-	55.3 ± 13.3	-	64.0 ± 16.8
PVR (Woods units)	-	12.8 ± 5.2	-	16.0 ± 6.4
mRAP (mm Hg)	-	7.9 ± 3.8	-	7.6 ± 4.0
CO (L/min)	-	4.0 ± 1.2	-	3.5 ± 0.5
6MWD (m)	-	401.7 ± 122.7	-	421.5 ± 123.4
NT-proBNP (pg/mL)	-	978.8 ± 1411.9	-	1690.9 ± 1461.9
Creatinine (μmol/L)	-	66.6 ± 11.5	-	68.5 ± 13.0
Bilirubin (μmol/L)	-	23.1 ± 23.9	-	24.6 ± 21.2
TAPSE (mm)	-	18.0 ± 4.1	-	16.0 ± 3.9
Drug therapy (%)				
PDE5 inhibitors	-	66.7	-	48.9
ERA	-	26.7	-	33.3
CCB	-	3.3	-	2.2
Prostanoids	-	6.7	-	13.3

BMI: body mass index; PAWP: pulmonary arterial wedge pressure; mPAP: mean pulmonary arterial pressure; PVR: pulmonary vascular resistance; mRAP: mean right atrial pressure; 6MWD: 6-minute walking distance; TAPSE: tricuspid annular plane systolic excursion; ERA: endothelin receptor antagonist; CCB: calcium channel blocker; IPAH: idiopathic pulmonary arterial hypertension; CO: cardiac output; PDE5: phosphodiesterase type 5; NT-proBNP: N-terminal pro-B-type natriuretic peptide.

Values are the mean ± standard deviation unless indicated otherwise.

Supplementary Table S2 All the 74 metabolites in HCs and patients with IPAH

Metabolite	HC (ng/mL)	IPAH (ng/mL)	Metabolite	HC (ng/mL)	IPAH (ng/mL)
Four Hydroxyl L roline	410.7±142	564.6±326.7	Nicotinamide	159.6±94.4	152.4±97.4
Five Methylthioadenosine	7.4±3.9	5±1.7	O Acetylcarnitine	808.8±301	1592.6±406.7*
Adenine	1.5±0.5	1.8±1.5	O Acetyl L serine	1021.8±535.9	2616.8±833.7*
Adenosine	1.5±2.2	2.4±9.7	Ornithine	1802.8±583.3	1413.2±321
AMP	23.4±19.7	6.9±2.4*	Phenylalanine	7885.5±1588.1	8082.9±1942.5
Arginine	1974.7±767.2	655.9±310.3*	Proline	22186.7±8703.2	23898.9±9292.6
Asparagine	928.2±281.8	646.3±181.2	Pyridoxine	0.2±0.1	0.1±0
Aspartate	134.9±92.6	118.8±38.6	Spermidine	423.5±238.3	155.4±74*
Biotin	158.1±74.9	146.2±106.3	Spermine	85.4±59.1	887.3±292.5*
Carnitine	7795.7±2280.5	10922.9±3318	Taurine	180.1±130.9	239.3±141.4
Carnosine	2.5±1.6	1.2±0.4	Thiamin	2.7±3.7	2.5±1.6
Choline	1387.3±653	3808.5±1297.6*	Threonine	3741.8±1503.1	2506.3±1046.8
Citrulline	1694.1±553.4	1140.2±280.2	Tryptophan	14748.2±3111.3	21389.2±6060.9
Creatine	8600.2±4463.4	8919.3±5636.1	Tyrosine	11556.8±3205.5	15833.6±4879
Creatinine	1558.4±594	7803.8±2266.9*	Valine	4595±1213	3645.7±1876.2
Cystamine	22953.3±15663.9	21838.9±11293.4	α Keto glutarate	218.8±73.6	138.2±82.3
Cysteine	157.1±254.1	126.9±144.6	Allantoin	284.9±127.6	222.1±152.3
Cystine	125.6±33.4	134.7±50	Benzoate	1199.9±1267.9	1693.6±2136.9
Cytosine	2.1±1	2±1.4	Citrate	1503.9±443.5	5306.9±2122.5*
dAMP	1.2±1.7	0.7±0.4	Cysteate	29±10.8	25.6±11.8
dCMP	7.8±12.6	2.3±0.7*	Deoxyuridine	55.8±18.3	53.2±31.6
Deoxyadenosine	0.2±0.1	0.1±0	Glutamate	1131.9±335.4	708.8±293.3
dGMP	9.7±12.9	3.7±1.3*	GMP	29.3±8.7	12.9±8.8*
Glutamine	22183.2±6194	18779.8±5019.9	Hippuric	2665.7±4342.2	2224.4±3473.3
Glycero 3 phosphocholine	1249.6±572.3	1022.4±434.1	Lactic	20064.4±8160.4	20241.8±8227.1
Guanine	21.6±28.5	7.4±6.3*	N acetyl L glutamate	19.2±8	13.7±4.9
Guanosine	90.5±42.3	72.2±25.3	N Acetylneuraminate	84.1±28.3	59.2±28
Histamine	5.3±2.2	4.6±1.9	Pantothenate	68.4±41.4	71.7±32
Homocysteine	1952±850.8	2338.4±856.4	Phenylacetylglycine	7.4±4.7	8.1±4.3
Hypoxanthine	1009.1±670.3	169.7±116.4*	Pyroglutamic acid	5758.9±1956	4455.8±1509.1
Inosine	296.8±209.6	168.5±193.8	Serine	1896.7±416.6	1218.4±369.4
Isoleucine	6483.5±1711.9	10247.2±3874.2	Succinate	1465.7±297.6	1346.6±496.8
Kynurenine	314±116.4	528.9±211.1	Thymine	5477.2±6866.6	35639.7±41481.2*
Leucine	28195.2±7147.6	33874.1±10876.8	Uric acid	43272.4±15645.7	15709.9±12196.4*
Lysine	756.1±459.9	392.5±152.5	Uridine	3424.1±1501.5	4070.8±2062.1

Methionine	2154.5±590.1	2902.4±775.1	Xanthine	291.2±131.2	356.3±172.6
N Acetylornithine	55.2±30.8	102.7±47.6*	Xanthosine	7.8±3	5.8±2.1

*$P < 0.05$, Student's t-test. Values are the mean ± standard deviation unless indicated otherwise.

Supplementary Table S3 Pathway enrichment analysis

Pathway name	**Hits**	***P***	**-log(*P*)**	**Holm *P***	**FDR**	**Impact**
Purine metabolism	6	1.00E-05	11.508	8.04E-04	8.04E-04	0.1391
beta-Alanine metabolism	3	5.85E-04	7.4446	4.62E-02	2.34E-02	0.08953
Arginine and proline metabolisms	4	1.01E-03	6.8967	0.078867	0.026963	0.15769
Glutathione metabolism	2	0.022393	3.799	1	0.44786	0.07064
D-arginine and D-ornithine metabolisms	1	0.04885	3.019	1	0.69475	0
Pyrimidine metabolism	2	0.052106	2.9545	1	0.69475	0.0722
Citrate cycle	1	0.11797	2.1374	1	1	0.06327
Nitrogen metabolism	1	0.21788	1.5238	1	1	0
Glycerophospholipid metabolism	1	0.21788	1.5238	1	1	0.0212
Histidine metabolism	1	0.24236	1.4173	1	1	0.0028
Glycine, serine, and threonine metabolisms	1	0.26143	1.3416	1	1	0
Glyoxylate and dicarboxylate metabolisms	1	0.2708	1.3064	1	1	0.00326
Aminoacyl-tRNA biosynthesis	1	0.37888	0.97053	1	1	0

FDR: false discovery rate

Supplementary Table S4 Primers for real-time PCR

Gene symbol	Species	Forward primer (5′–3′)	Reverse primer (5′–3′)
PRR23A	human	GTTTCACCCCTACTCTTGCT	TTCCAAAAGGTCCAGTGCAT
CTFR	human	TAGCTTCCTATGACCCGGAT	TATCTAGAACACGGCTTGACA
ADAMT14	human	TCTGTGTACTGCCCCGTGAC	GCATCACAGCCCCAAACGA
CD9	human	CTATGGCTCCGATTCGACT	GCTCCGATCAGAATATAGACTCC
ERG	human	AACAAGAGAAAAGACACGAGA	CTTTTAGTTCATAGTCCCGGTA
FGFR4	human	TCCTTGACCTCCAGCAACGAT	CGAATGCCTCCAATGCGGTTC
GCLM	human	CAGATGTCTTGGAATGCACT	CCAGTAAGGCTGTAAATGCTC
HR	human	CCTGTGCCCCTTTTCATGGTA	GTTGTTTAAGCCAGAATGATTCCC
MICALCL	human	TATTCACCGAGCTGATGCAAG	ACAGCCTCTGGAGAATACGAA
RFX8	human	CTTTAAATGCTACGACGTCCA	TGACTTCAAAACGCTGACAC
RNF128	human	AGCCGTCATCTTTAACTTCCC	TTGCATTCCGTAGCCTTCGAG
TCF7	human	ATGGTCACAAGCACAAAGCTCA	CTCCCCAATTTGCCTGATAAGGT
ZNF214	human	GAAAACCTCTGTCAATGCTCC	CATGAAGTACTGAACTCCGAT
ZNF467	human	TGCCCACACAGAACAAGC	TTCTGCCTCCTGATCTTCGT
GAPDH	human	TCTGACTTCAACAGCGACACC	AGCCAAATTCGTTGTCATACCAG

Supplementary References

1. Galiè, N. et al. 2015 ESC/ERS Guidelines for the diagnosis and treatment of pulmonary hypertension: The Joint Task Force for the Diagnosis and Treatment of Pulmonary Hypertension of the European Society of Cardiology (ESC) and the European Respiratory Society (ERS): Endorsed by: Association for European Paediatric and Congenital Cardiology (AEPC), International Society for Heart and Lung Transplantation (ISHLT). *Eur. Heart J.* **1**, 67–119 (2015).

2. Wang, Z., Zhang, J., Ren, T., & Dong, Z. Targeted metabolomic profiling of cardioprotective effect of Ginkgo biloba L. extract on myocardial ischemia in rats. *Phytomedicine* **6**, 621–631 (2016).

3. Rothman, A. et al. Development and characterization of a cloned rat pulmonary arterial smooth muscle cell line that maintains differentiated properties through multiple subcultures. *Circulation* **6,** 1977–1986 (1992).

4. Zeng, Y. et al. CXCR1 and CXCR2 are novel mechano-sensors mediating laminar shear stress-induced endothelial cell migration. *Cytokine* **1**, 42–51 (2011).

5. Ahmad, I. et al. Sleeping Beauty screen reveals Pparg activation in metastatic prostate cancer. *Proc. Natl. Acad. Sci. USA* **29**, 8290–8295 (2016).

6. Fan, Y. F. et al. The phosphodiesterase-5 inhibitor vardenafil reduces oxidative stress while reversing pulmonary arterial hypertension. *Cardiovasc. Res.* **3**, 395–403 (2013).

7. Ma, W. et al. Calpain mediates pulmonary vascular remodeling in rodent models of pulmonary hypertension, and its inhibition attenuates pathologic features of disease. *J. Clin. Invest.* **11**, 4548–4566 (2011).